Mitochondrial fusion is frequent in skeletal muscle and supports excitation–contraction coupling

Verónica Eisner,[1] Guy Lenaers,[2] and György Hajnóczky[1]

[1]MitoCare Center, Department of Pathology, Anatomy, and Cell Biology, Thomas Jefferson University, Philadelphia, PA 19107
[2]Institut national de la santé et de la recherche médicale (INSERM) U1051, Institut des Neurosciences de Montpellier, 34091 Montpellier, France

Genetic targeting experiments indicate a fundamental role for mitochondrial fusion proteins in mammalian physiology. However, owing to the multiple functions of fusion proteins, their related phenotypes are not necessarily caused by altered mitochondrial fusion. Perhaps the biggest mystery is presented by skeletal muscle, where mostly globular-shaped mitochondria are densely packed into the narrow intermyofilamental space, limiting the interorganellar interactions. We show here that mitochondria form local networks and regularly undergo fusion events to share matrix content in skeletal muscle fibers. However, fusion events are less frequent and more stable in the fibers than in nondifferentiated myoblasts. Complementation among muscle mitochondria was suppressed by both in vivo genetic perturbations and chronic alcohol consumption that cause myopathy. An Mfn1-dependent pathway is revealed whereby fusion inhibition weakens the metabolic reserve of mitochondria to cause dysregulation of calcium oscillations during prolonged stimulation. Thus, fusion dynamically connects skeletal muscle mitochondria and its prolonged loss jeopardizes bioenergetics and excitation–contraction coupling, providing a potential pathomechanism contributing to myopathies.

Introduction

Adult skeletal muscle (SM) fibers show highly organized structure, in which most of the mitochondria appear as an array of isolated organelles (Vendelin et al., 2005) densely packed into the space among the myofilaments and physically interact with the sarcoplasmic reticulum (SR; Ogata and Yamasaki, 1997; Boncompagni et al., 2009; Eisner et al., 2013). Mitochondria display diverse orientation and communication with the SR among different species, fiber types, and differentiation stages; extensive SR-to-mitochondria contacts are distinctive for mammals (Franzini-Armstrong and Boncompagni, 2011).

Mitochondria provide a major ATP source for contraction and also participate in Ca^{2+} buffering. Furthermore, localization of mitochondria close to the SR promotes local delivery of Ca^{2+} transients mediating the excitation–contraction (EC) coupling to the mitochondrial matrix (Rizzuto et al., 1994; Brini et al., 1997; Pacher et al., 2002; Rudolf et al., 2004; Rogers et al., 2007) to activate the Ca^{2+}-sensitive mitochondrial matrix dehydrogenases (CSMDHs; Hajnóczky et al., 1995; Robb-Gaspers et al., 1998), and in turn, enhance ATP production (excitation–oxidative metabolism coupling; Jouaville et al., 1999).

Emerging evidence supports that functionally competent mitochondria are maintained by continuous remodeling in many cell types. Remodeling is achieved by the breakdown of damaged components or even whole mitochondria (Lemasters, 2005; Tatsuta and Langer, 2008; Twig et al., 2008; Karbowski and Youle, 2011) and by replacing them with functional ones. The latter process is effectively supported by fusion and complementation among individual mitochondria (Ono et al., 2001; Detmer and Chan, 2007; Lackner and Nunnari, 2009). Mitochondrial fusion has different modes, including transient fusion or kiss-and-run, which allows complementation of only soluble components, and complete fusion that supports mixing of all components of the merging mitochondria (Liu et al., 2009). In mice, SM-specific depletion of the outer mitochondrial membrane (OMM) fusion protein, Mfn1/2, impairs mtDNA integrity and metabolic capacity (Chen et al., 2010). Furthermore, patients carrying a mutation of the inner mitochondrial membrane (IMM) fusion protein,

Correspondence to György Hajnóczky: gyorgy.hajnoczky@jefferson.edu

Abbreviations used in this paper: 2P, two photon; ADOA, autosomal-dominant optical atrophy; CRU, Ca^{2+} release unit; CSMDH, Ca^{2+}-sensitive mitochondrial matrix dehydrogenase; EC, excitation–contraction; ECM, extracellular medium; ES, electrical stimulation; EtOH, ethanol; FDB, flexor digitorum brevis; IMM, inner mitochondrial membrane; jSR, junctional sarcoplasmic reticulum; KO, knockout; MEF, mouse embryonic fibroblast; OMM, outer mitochondrial membrane; SM, skeletal muscle; SR, sarcoplasmic reticulum; TT, transversal tubule; WT, wild type.

The Rockefeller University Press $30.00
J. Cell Biol. Vol. 205 No. 2 179–195
www.jcb.org/cgi/doi/10.1083/jcb.201312066

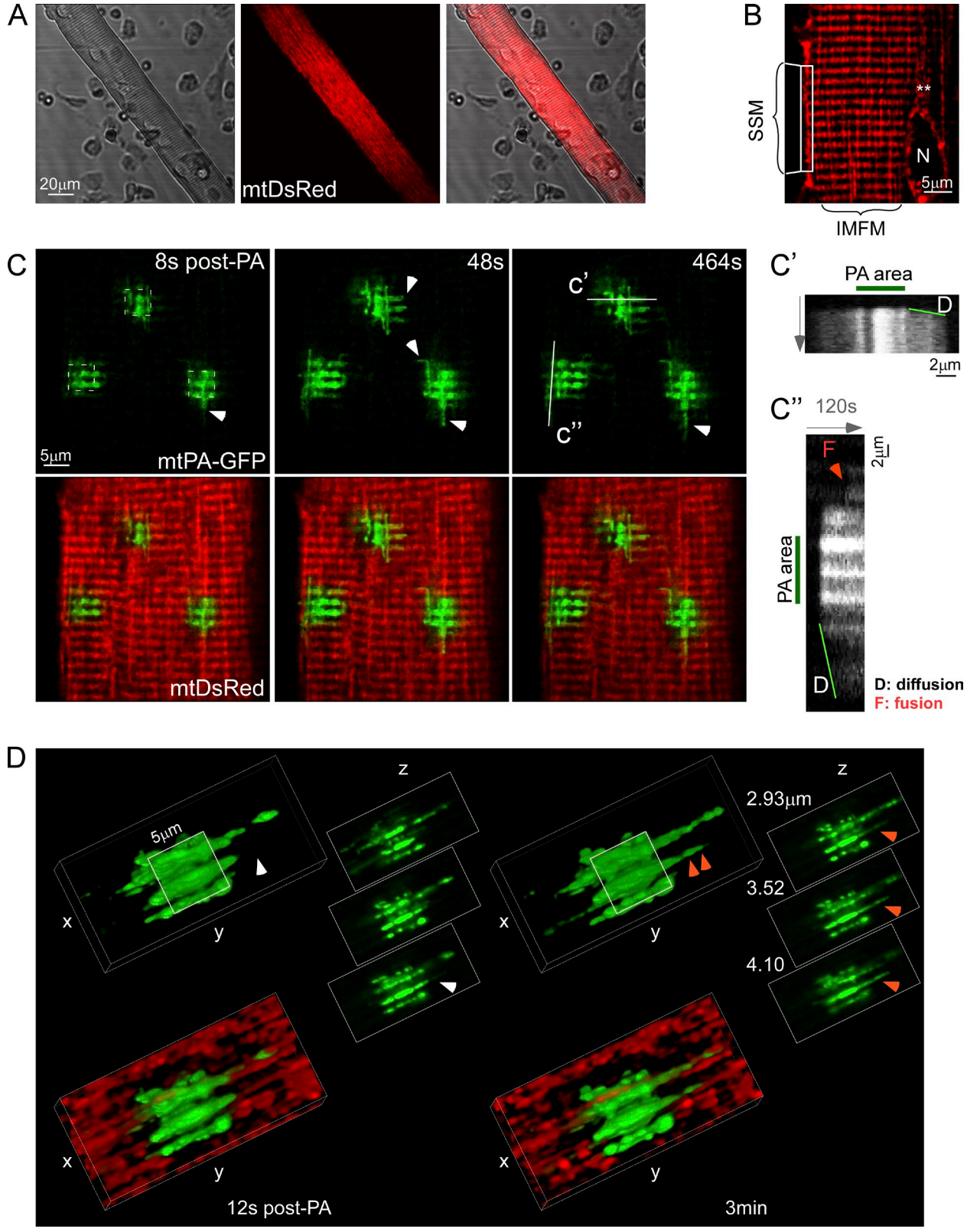

Figure 1. **Local mitochondrial networks in FDB fibers.** (A) An isolated fiber (left) expressing mtDsRed (center). (B) Mitochondrial distribution. Specific subgroups of mitochondria are indicated. IMFM, intermyofibrillar mitochondria; N, nucleus; SSM, subsarcolemmal mitochondria; **, perinuclear mitochondria. (C) Image time series showing a representative FDB fiber before and after 2P photoactivation of mtPA-GFP (white dashed squares). Arrowheads show sites of diffusion, D, of mtPA-GFP into neighboring mitochondria. Line-scan images further illustrate transversal (c') and longitudinal (c") diffusion, D, of mtPA-GFP through interconnected mitochondria starting immediately after photoactivation and expanding continually, and a fusion event (F, orange arrowhead) appearing at a later time point as an abrupt expansion of the PA-GFP signal. (D) 3D reconstruction of a photoactivated area a few seconds (left) and 3 min after photoactivation (right) to illustrate matrix continuity and discrete mixing events (orange and white arrowheads), respectively. Notably, the discrete event could not be caused by mitochondrial movement because the mtPA-GFP and mtDsRed fluorescence changes had opposite directions (not depicted).

Opa1, associated with autosomal-dominant optical atrophy (ADOA), develop late onset myopathy (Yu-Wai-Man et al., 2010) and altered muscle mitochondrial ATP synthesis (Lodi et al., 2011). Mitochondria were early proposed to be energy-transmitting cables in neonatal cardiomyocytes (Amchenkova et al., 1988), and growing evidence illuminates a role for mitofusins in the heart (Chen et al., 2011; Papanicolaou et al., 2011). However, mitochondrial fusion proteins have multiple functions, including a contribution of Opa1 to cristae remodeling (Frezza et al., 2006) and of Mfn2 to stabilizing interactions between mitochondria and SR/ER (de Brito and Scorrano, 2008; Chen et al., 2012). Thus, it is not possible to infer from the phenotypes of fusion protein deletions/mutations the relevance of mitochondrial fusion without direct assessment of the fusion activity. However, this task has remained difficult in the tissues most dependent on mitochondrial energy production like the SM. An important motivation for our study was to visualize and quantitate mitochondrial fusion dynamics in SM.

The biological relevance of fusion goes well beyond the maintenance of energy homeostasis. Dynamical restructuring of the mitochondria might be important for cell signaling, including Ca^{2+} signaling that directly controls the contractile function. Fragmentation of mitochondria causes alterations in both cytoplasmic and mitochondrial Ca^{2+} transients (Frieden et al., 2004; Szabadkai et al., 2004; Eisner et al., 2010), and damaged mitochondria favor the propagation of abnormal cytoplasmic Ca^{2+} waves in muscle fibers of an amyotrophic lateral sclerosis mouse model (Zhou et al., 2010). Also, Ca^{2+} is a significant second messenger in the regulation of mitochondrial fission by promoting Drp1 localization to the OMM (Hom et al., 2007; Cereghetti et al., 2008). Therefore, a second important goal for our work was to assess mitochondrial fusion dynamics in the context of SM Ca^{2+} signaling.

We adapted the fluorescent photo-activated protein technology to the study of mitochondrial fusion dynamics in adult SM fibers. Our study describes the adaptation of the fusion machinery to the special structural organization presented by the SM. Furthermore, combining the analysis of fusion dynamics with genetic perturbations and functional studies, this work explores the relevance of fusion activity in the maintenance of bioenergetics and Ca^{2+} signaling in normal muscle and in the dysfunction caused by ADOA-associated Opa1 mutants and chronic alcohol exposure.

Results

Mitochondrial continuity in adult SM

To evaluate whether mitochondria in adult SM display any level of continuity and undergo interorganellar fusion events, we transfected the flexor digitorum brevis (FDB) muscle of adult rats by in vivo electroporation with cDNA encoding mitochondrial matrix-targeted DsRed (mtDsRed) and photoactivatable GFP (mtPA-GFP). After 7–10 d, the muscles were harvested and digested to obtain isolated fibers expressing the fluorescent proteins (Fig. 1 A). MtDsRed was expressed in all different populations of mitochondria, specifically intermyofibrillar, subsarcolemmar, and perinuclear organelles (Fig. 1 B). We focused our study on intermyofibrillar mitochondria because this is the subpopulation of organelles that physically interacts with the terminal cisternae of the SR (Boncompagni et al., 2009), accumulates Ca^{2+} upon RyR1 activation (Shkryl and Shirokova, 2006), and buffers osmotic shock-induced Ca^{2+} sparks (Rossi et al., 2011), making them particularly relevant for the Ca^{2+} homeostasis regulation associated with the Ca^{2+} release units (CRUs) and the EC coupling. Using confocal microscopy, time series of fluorescence images were recorded and 25-μm^2 square-shaped areas were illuminated by a pulsed laser to photoactivate mtPA-GFP in two-photon (2P) mode. Mitochondrial matrix is predominantly composed of soluble proteins that show rapid diffusion (Partikian et al., 1998). Mitochondrial matrix continuity is unveiled by the diffusion of the photoactivated PA-GFP to the regions outside the 2P illuminated area. Fig. 1 C and Video 1 show that as early as 8 s after 2P illumination started, mtPA-GFP diffused toward the surrounding area of the photoactivated box and farther to reach a set of discrete interconnected mitochondria. Matrix connectivity occurs in both longitudinal and transversal directions, as shown by arrowheads and line-scan analysis in Fig. 1, C′ and C″, and in 3D reconstruction (Fig. S1 A). Longitudinal diffusion of mtPA-GFP can reach distances involving as much as 2–3 sarcomeres (6 µm), as shown by the sets of double rows of mitochondria that run parallel to the fiber's I-band, as described previously (Boncompagni et al., 2009). Furthermore, line-scan analysis also shows at later time points abrupt, single-step spreading of PA-GFP fluorescence between two neighboring organelles, which likely reflects a fusion event (Fig. 1 C″, orange arrowhead). Thus, the mtPA-GFP diffusion reveals both discrete subsets of organelles with preset matrix continuity and de novo fusion events.

To visualize mitochondrial continuity in 3D, z-series of images was collected at two different time points after PA-GFP photoactivation. Fig. 1 D shows mtPA-GFP spreading beyond the photoactivation limits 12 s after photoactivation mostly in the longitudinal direction (left), and the appearance of a new organelle 3 min later, probably due to a fusion event (right, double arrowhead). High magnification 3D reconstruction of mitochondria in an FDB fiber reveals a complex array involving interconnected longitudinal and horizontal structures (Fig. S1 A). Interestingly, some of the connections appear as narrow structures, suggesting the presence of specialized material transfer domains (Fig. S1 A, white arrows) that keep longitudinal organelles continuously communicated, despite the restrictive myofibrillar architecture. These domains are further evidenced by means of matrix content transfer by the mtPA-GFP diffusion kinetics along single tubular organelles after photoactivation (Fig. S1 B). The elongated organelles that show a narrowing of their structure present slower mtPA-GFP diffusion kinetics (Fig. S1 B, right) than tubular mitochondria with a constant diameter (Fig. S1 B, left). Up to this point, our data demonstrate that mitochondria in adult SM fibers display stable connections of varying size and direction, which allow exchange of soluble matrix content.

Mitochondrial fusion dynamics in SM fibers

To validate fusion events, reciprocal spreading of mtPA-GFP and mtDsRed among mitochondria that were not continuous at the time of PA-GFP photoactivation was sought. Fig. 2 A shows a

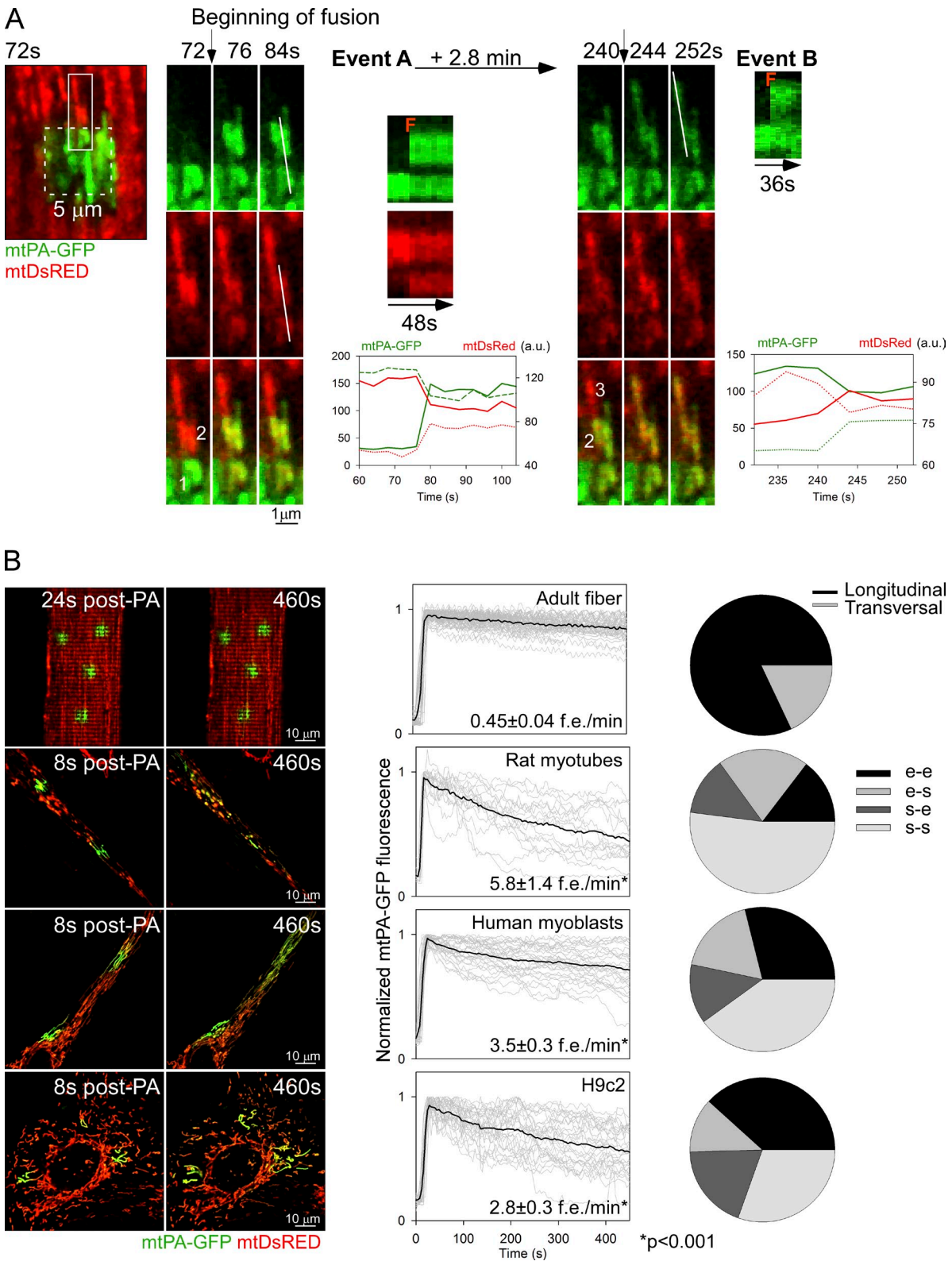

Figure 2. **Mitochondrial fusion events in FDB fibers.** (A) FDB fiber expressing both mtDsRed and mtPA-GFP. During photoactivation of mtPA-GFP, mtDsRed is photobleached, allowing detection of the mixing of each fluorescent protein after mitochondrial fusion. Left image shows the photoactivation area (white dashed box) and its surrounding region 72 s after 2P photoactivation. Mitochondria shown in the white rectangular box undergo two sequential longitudinal fusion events at 76 s and 244 s, respectively. Event A: mitochondrion 1 donates fluorescent mtPA-GFP to mitochondrion 2 (acceptor) abruptly at 76 s. At the same time the green acceptor mitochondrion donates fluorescent mtDsRed to mitochondrion 1. Line scans also show the abrupt and complementary intermitochondrial transfer of the fluorescent proteins (F). Subsequently, 2.8 min later, mitochondrion 2 fuses with mitochondrion 3 (event B, 244 s). The line scan is only shown for the green color because of the relatively small gradient in the red fluorescence. Bottom plots show mtPA-GFP and mtDsRed mixing kinetics of each mitochondrion that undergoes fusion. Continuous line, PA-GFP accepting organelles; dashed lines, PA-GFP donating organelles.

representative example where three individual mitochondria that were originally not connected are undergoing two sequential fusion events. 2P photoactivation of PA-GFP is confined to mitochondrion 1 and is accompanied by mtDsRed photobleaching in the same organelle (Fig. 2 A, "72 s" images). 76 s after photoactivation (event A), 1 donates photoactivated PA-GFP to mitochondrion 2, until reaching an equilibrium. At the same time, mitochondrion 2 shares its fluorescent mtDsRed with 1, leading to red photorecovery in 1. The graph shows the time-course of rapid and simultaneous equilibration of the PA-GFP and DsRed fluorescence between 1 and 2. A few minutes later, mtPA-GFP fluorescence spreads from 2 to mitochondrion 3 as a discrete step, indicating a second fusion event (event B). The movie version of these fusion events is shown in Video 1 (bottom photoactivated area). In some cases, merge of a single mitochondrion with a complex mitochondrial network was also documented (Fig. S2 A). These data provide direct evidence that mitochondria in adult SM are connected dynamically by fusion events that support rapid exchange of soluble matrix content.

Next, the fusion events were quantitatively analyzed in adult FDB muscle fibers, and muscle progenitor cells: primary rat myotubes derived from the FDB muscle, human differentiating myoblasts, and H9c2 cardiac myoblasts (Fig. 2 B). The rat myotubes and human differentiating myoblasts show an elongated shape like the fibers but do not have precisely organized myofilaments to limit the mitochondrial dynamics (images on the left). The progression of the distribution of PA-GFP fluorescence between the images collected within the first 30 s and 7 min after photoactivation indicates less mitochondrial fusion activity in the fibers than in the less differentiated models (Fig. 2 B, left). The size and mitochondrial content of the different cell types is different, therefore the fusion count was normalized for three photoactivation areas in each. Adult fibers display 0.45 ± 0.04 events/min, whereas rat myotubes and human differentiating myoblasts show 13 and 8 times more, respectively (Fig. 2 B, middle). H9c2 cells also display a high mitochondrial fusion rate consistent with our previous study (Liu et al., 2009). The cell type–specific difference in mitochondrial fusion activity is also apparent in the graphs showing the time-dependent loss of mtPA-GFP fluorescence in the photoactivation area. FDB fibers show slower decay kinetics compared with any of the less differentiated muscle cells (Fig. 2 B, graphs in central panel). As to the orientation, adult fiber mitochondria predominantly present fusion events in the longitudinal axis (82%; Fig. 2 B, right). However, transversally oriented events are also present (18%; see example in Fig. S2 B). By contrast, rat myotubes and human differentiating myoblasts present a significantly higher percentage of mitochondria lateral fusion events (side-to-side manner). For an example of the relatively fast fusion dynamics and mostly lateral orientation of fusion events in a rat myotube, see Video 2. Finally, H9c2 myoblasts display a diverse spatial pattern of fusion events, which can be attributed to a less organized architecture. Mitochondria show ample movement and fusion events followed by rapid separation of the interacting organelles (kiss-and-run fusion) in H9c2 myoblasts (47%; Liu et al., 2009) and, also in human myoblasts and rat myotubes, 14 and 24%, respectively. The dynamic interactions among mitochondria in less differentiated muscle cells are supported by both mitochondrial fusion and motility. However, in adult fibers, directional mitochondrial movements seldom occur due to spatial restrictions, and rapid termination of fusion events by fission is visible infrequently, only 0.15 fission events/fiber ($n = 45$). Although the number of fusion events is expected to be matched by the number of fission events, the rate of spreading normalized to the number of fusion events is 2–3 times higher in the fibers than in the myoblasts or myotubes (Fig. 2 B, middle), indicating that the lifetime of fusion events is relatively long in adult fibers. Thus, adult SM mitochondria show fusion events regularly but the amount is less than that in the progenitor cells. In addition, due to the spatial order and confinement, mitochondria in adult muscle fibers can engage in mostly long-lasting longitudinal fusion events, which likely provide opportunity for effective and prolonged content exchange.

ADOA-associated Opa1 mutations suppress mitochondrial fusion in SM

Genetic alterations of mitochondrial fusion proteins have been shown to perturb mitochondrial function in the SM and to be associated with myopathy (Chen et al., 2010; Lodi et al., 2011). However, whether these changes are actually based on inhibition of mitochondrial fusion is an open question. To explore this possibility, ADOA-associated Opa1 mutations, Opa1G300E and Opa1 Δ58 (Olichon et al., 2007), were introduced together with mtDsRed and mtPA-GFP to the FDB muscle of normal adult rats. PA-GFP diffusion after photoactivation is inhibited in G300E- and Δ58 Opa1-expressing fibers (Fig. 3 A, images), suggesting a decrease in mitochondrial matrix continuity. Furthermore, mitochondrial fusion is also significantly inhibited by each mutant (Fig. 3 A, bottom). Thus, interference with the conserved IMM fusion machinery using ADOA-associated Opa1 mutations causes inhibition of mitochondrial fusion dynamics in the adult SM.

Mfn1 but not Mfn2 silencing inhibits mitochondrial fusion in SM

We next evaluated the respective contribution of the two OMM fusion proteins, Mfn1 and Mfn2 GTPases to SM fusion dynamics. In vivo cotransfection with either Mfn1 or Mfn2 siRNA and mt-DsRed and mtPA-GFP was followed by isolation of FDB fibers, 6 d after electroporation (Fig. 3 B). Immunoblotting confirmed the presence of both Mfn1 and Mfn2 in the mitochondria and an effective depletion of each by isoform-specific siRNA

A single representative example is shown out of 333 events from more than 5 experiments. (B) Fusion event rate and orientation characteristics in different muscle cells. Left: representative images of mtPA-GFP diffusion within the first 8–24 s of photoactivation and further spreading after 8 min. Middle: mtPA-GFP fluorescence decay evaluated inside the photoactivation area. Gray curves, individual regions; black curves represent the mean curves. The fusion events rate is also indicated for each cell type (FDB fibers, $n = 333$ events, 86 cells; rat myotubes, $n = 123$ events, 5 cells; human differentiating myoblasts, $n = 309$, 15 cells; and H9c2 myoblasts, $n = 209$, 10 cells). Right: orientation distribution of the fusion events in each cell type. e-e, end to end; e-s, end to side; s-e, side to end; s-s, side to side.

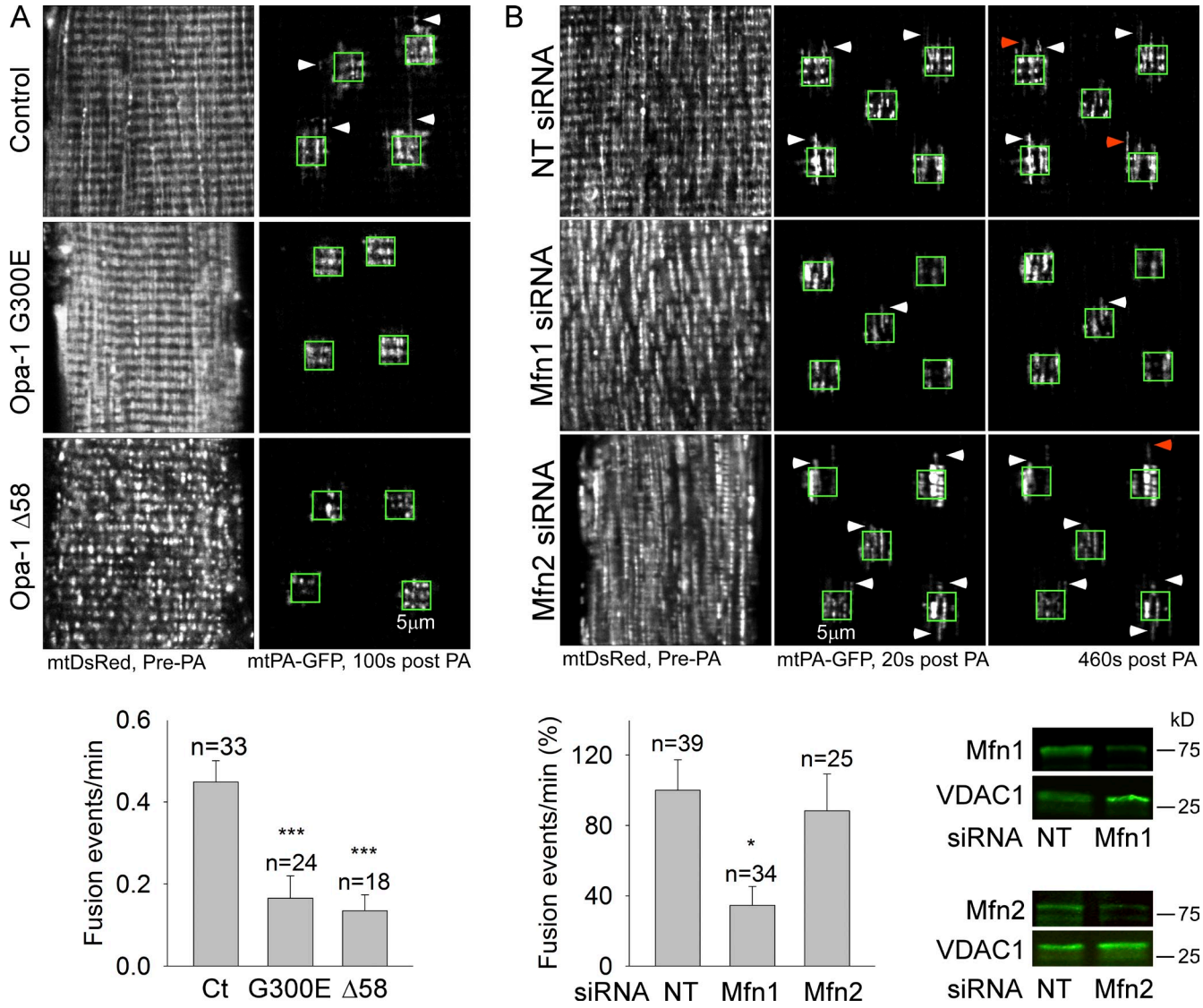

Figure 3. **ADOA-associated Opa1 mutations and Mfn1 silencing inhibit mitochondrial fusion in FDB fibers.** (A) Opa1 mutants G300E (GTPase domain) or Δ58 (deletion of the GTPase effector domain) were expressed in FDB muscles together with mtDsRed and mtPA-GFP. Top: examples of the general structure of mitochondria (mtDsRed) before 2P illumination within green boxes, and discrete mitochondrial networks 100 s after photoactivation (mtPA-GFP, white arrowheads), in control and FDB fibers expressing mutant Opa1. Bottom: bar charts show the frequency of fusion events for each condition (2 rats/condition; ***, $P < 0.001$). (B) Nontargeting (NT) siRNA and Mfn1 or Mfn2 were coexpressed with mtDsRed and mtPA-GFP in FDB muscles. Top: representative images of the mtPA-GFP diffusion (white arrowheads) and fusion events (orange arrowheads). Bar chart displays the fusion event rates (Mfn1siRNA = 3 rats; *, $P < 0.05$; Mfn2 siRNA = 2 rats). Bottom right: Mfn1 and Mfn2 Western blots of mitochondria isolated from FDB after siRNA treatment.

(Fig. 3 B, bottom right). Fig. 3 B shows that silencing of Mfn1 protein, but not Mfn2, leads to decreased mitochondrial continuity (top, representative images) and lesser mitochondrial fusion rate (bottom left). Thus, the dominant OMM fusion protein in SM, at least in the FDB, seems to be Mfn1.

Short-term inhibition of mitochondrial fusion does not alter intracellular Ca^{2+} regulation in SM

Fig. 3 showed that ADOA-associated Opa1 mutations and Mfn1 silencing cause inhibition of SM mitochondrial fusion. Human mutations of IMM and OMM fusion proteins (ADOA and Charcot-Marie-Tooth disease) are commonly associated with myopathy, manifesting muscle weakness (Yu-Wai-Man et al., 2010; Feely et al., 2011; Vital and Vital, 2012), and knockout of the OMM fusion proteins in mouse SM is detrimental for the metabolic performance of the mitochondria (Chen et al., 2005, 2010). Therefore, we evaluated whether interference with mitochondrial fusion alters SM EC coupling–associated Ca^{2+} transients, the trigger of muscle contraction (Westerblad et al., 1991), as well as their metabolic target, the CSMDH.

Contractions are directly proportional to the $[Ca^{2+}]_c$ transients that can be documented by Fura2. We tested the $[Ca^{2+}]_c$ transients induced by repetitive tetanic stimulation in FDB fibers expressing Opa1G300E or Mfn1 siRNA. Interestingly, neither the transient overexpression of Opa1G300E nor short-term silencing of Mfn1 in FDB fibers alters significantly the $[Ca^{2+}]_c$ responses to repetitive tetanic stimulation (Fig. S3 and Fig. 4 A, respectively).

As to CSMDH activity, we managed to set up monitoring NAD(P)H fluorescence simultaneously with recording $[Ca^{2+}]_c$ transients with RCaMP (Akerboom et al., 2013) in FDB muscle fibers. Fig. 4 B shows a transient increase of mitochondrial NAD(P)H levels closely following the repetitive $[Ca^{2+}]_c$ transients, which reaches its maximum 25.9 ± 1.9 s after the start of the repetitive tetanic electrical stimulation (ES; $n = 14$). Notably, in these measurements a bleed-through between the RCaMP and NAD(P)H fluorescence caused the individual $[Ca^{2+}]_c$ spikes to appear on the top of the NAD(P)H signal. Therefore, the NAD(P)H transient was also validated by NAD(P)H measurement in fibers not expressing RCaMP (Fig. S4). The NAD(P)H signal induced by repetitive tetanic ES is not significantly attenuated by short-term Mfn1 silencing (Fig. 4 B).

Prolonged Mfn1 depletion interferes with RyR1-mediated Ca^{2+} oscillations

We speculated that long-term interference with mitochondrial fusion might cause progressive problems with calcium signaling and energy metabolism. Unfortunately, long-term expression of Opa1 mutants or Mfn1 siRNA in SM is difficult. To assess the effect of chronic Mfn1 down-regulation on repetitive activation of Ca^{2+} signaling, we expressed RyR1, the SM-specific isoform of the Ca^{2+} release channel in wild-type (WT) and Mfn1 knockout (KO) mouse embryonic fibroblasts (MEFs), which are devoid of significant expression of any RyRs. Notably, the MEFs were also appealing because their mitochondrial fusion activity seems to be primarily on Mfn1 (Chen et al., 2005) like we found it in SM.

Upon treatment with caffeine, $[Ca^{2+}]_c$ oscillations are triggered only in the RyR1-expressing cells (unpublished data). Fig. 5 shows that many WT cells display regular $[Ca^{2+}]_c$ oscillations (Fig. 5 A), whereas Mfn1KO cells show a decay in the amplitude (Fig. 5, A–C), as well as fewer $[Ca^{2+}]_c$ transients (Fig. 5 C). Also, Mfn1 KO cells showed progressive Ca^{2+}-induced loss of the mitochondrial membrane potential that was measured simultaneously with $[Ca^{2+}]_c$ as a generic measure of the mitochondrial energy metabolism (Fig. 5 D).

Next, we compared the effect of short-term silencing of Mfn1 in WT MEF cells with the prolonged depletion in Mfn1KO cells. Fig. 5 E shows that the Ca^{2+} oscillation decay observed on the Mfn1KO cells is not phenocopied in Mfn1-silenced WT cells, and that the rescue of mitochondria morphology by re-expression of Mfn1 in Mfn1KO cells (not depicted) was not enough to restore sustained RyR1-mediated $[Ca^{2+}]_c$ oscillations upon caffeine stimulation.

During $[Ca^{2+}]_c$ oscillations, WT MEFs show an increase in NAD(P)H fluorescence that is greatly suppressed in Mfn1KO cells (Fig. 5 F). WT MEFs with short-term Mfn1 silencing also have some decrease in the NAD(P)H response, whereas short-term Mfn1 expression in the KO is not enough to rescue the NAD(P)H response during RyR1-mediated $[Ca^{2+}]_c$ oscillations (Fig. 5 F). Thus, long-term loss of Mfn1 causes a decay in RyR1-dependent $[Ca^{2+}]_c$ oscillations, impaired NAD(P)H, and delta psi generation. Short-term silencing of Mfn1 and short-term rescue do not phenocopy the Mfn1 KO and WT, respectively. Because loss of Mfn1 (1) alters mitochondrial continuity and fusion (Fig. 3 B) but causes no change in the SR ultrastructure (Chen et al., 2012), (2) does not affect the onset of $[Ca^{2+}]_c$ oscillations (Figs. 4 and 5), and (3) seems to affect mitochondrial metabolism earlier than $[Ca^{2+}]_c$ oscillations (Fig. 5 F), it is plausible that the crippled mitochondrial quality control in Mfn1-deficient cells first impairs energy metabolism, which in turn is affecting $[Ca^{2+}]_c$ oscillations. Importantly, previous studies have documented that inhibition of mitochondrial metabolism causes decay of $[Ca^{2+}]_c$ oscillations (Jouaville et al., 1995; Pacher et al., 2002). This is because mitochondria are strategically localized close to RyRs, and their metabolic dysfunction affects local Ca^{2+} buffering and ATP supply, both of which are needed for repetitive activation of RyRs and SR/ER Ca^{2+} ATPase (SERCA).

Chronic EtOH exposure inhibits mitochondrial fusion and lowers Mfn1 protein levels

In addition to diseases initiated by a genetic defect, mitochondrial morphology and function seem to be a main target of environmental cues, too. For example, mitochondrial ultrastructure damage is apparent in the SM of alcoholics (Song and Rubin, 1972) and mitochondria and their quality control are considered to be a primary target of chronic alcohol exposure (Mitchell et al., 2013). Inhibition of mitochondrial fusion dynamics has been observed during chronic ethanol (EtOH) exposure in hepatocytes, the primary sites of EtOH metabolism (Das et al., 2012). Whether chronic EtOH impairs SM mitochondrial dynamics to impair EC coupling is unclear. Here, we used FDB from EtOH-fed rats as a model to test whether environmental factors can modulate fusion dynamics in SM. Rats were fed with a 36% EtOH diet for 6–11 mo (Das et al., 2012). Diffusion of photoactivated mtPA-GFP is attenuated (Fig. 6 A, white arrowheads) and the fusion rate is decreased by 50% in FDB muscle harvested from EtOH-fed rats relative to pair-fed control (bar chart). To expose the underlying mechanism, we evaluated the mitochondrial fusion protein levels in SM mitochondria isolated from control and EtOH-fed rats. Neither Mfn2 nor Opa1 protein levels change consistently; however, Mfn1 shows a significant decrease (Fig. 6 B; $P < 0.001$, $n = 12$ independent pairs). Therefore, we aimed to rescue the decreased mitochondrial continuity by overexpression of Mfn1. Fig. 6 C shows that expression of full-length Mfn1 in the FDB muscle of EtOH-fed rats significantly increased the diffusion of mtPA-GFP outside the photoactivation area, compared with non-rescued fibers. Taken together, these data demonstrate that chronic EtOH consumption causes inhibition of mitochondrial fusion in SM. This effect might be due at least in part to down-regulation of Mfn1. To our knowledge, this experiment represents the first in vivo rescue of mitochondrial dynamics in a differentiated cell.

Chronic EtOH exposure impairs SM $[Ca^{2+}]_c$ regulation

A common consequence of chronic alcohol abuse is myopathy (Fernández-Sola et al., 2000). Therefore, we evaluated whether the Ca^{2+} transients mediating EC coupling were perturbed in the fibers coming from the EtOH-fed animals. Neither resting $[Ca^{2+}]_c$ nor the maximum amplitude of the first 10 transients is significantly affected by EtOH feeding. By contrast, $[Ca^{2+}]_c$ transients decay rapidly in the fibers coming from the EtOH-fed animals

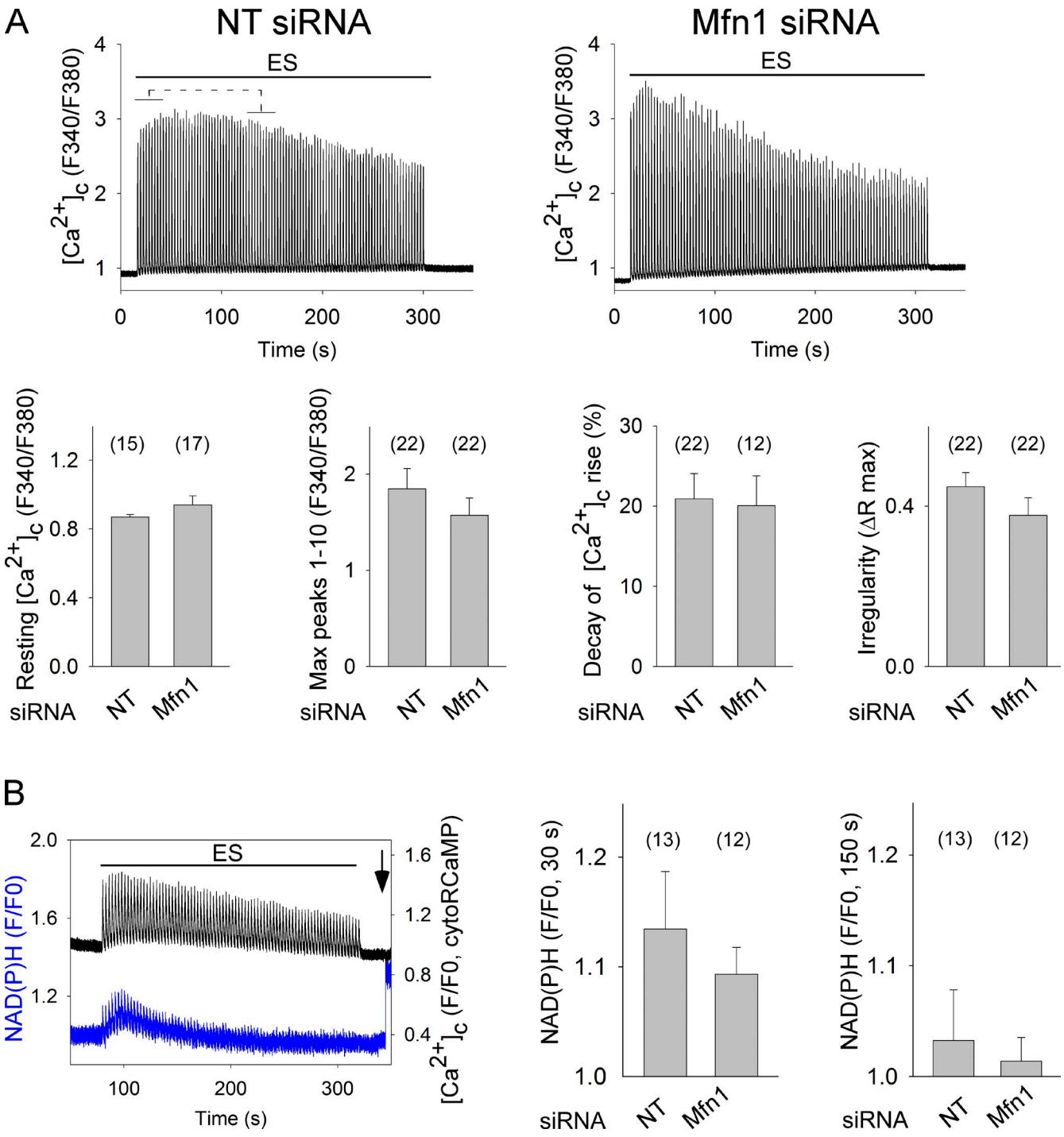

Figure 4. **Short-term silencing of Mfn1 does not alter trains of $[Ca^{2+}]_c$ transients and activation of the CSMDH in SM fibers.** (A) FDB muscles were cotransfected with mtDsRed and NT or Mfn1siRNA. After 7–10 d, fibers were isolated and loaded with Fura2. mtDsRed-positive fibers that responded to single electric pulses were picked. Fibers were challenged by repetitive tetanic ES. Top: representative $[Ca^{2+}]_c$ transients. Bottom bar charts show from left to right: $[Ca^{2+}]_c$ levels preES, max amplitude (peaks 1–10), the $[Ca^{2+}]_c$ transient amplitude decay for the time period indicated by brackets above the representative traces (([mean peaks 1–10] − [mean peaks 30–40])/[mean peaks 1–10] × 100), and irregularity in amplitude of the $[Ca^{2+}]_c$ transients (max − min)/max, among peaks 1–100 ($n \geq 4$ rats, the number of fibers is shown in the bar charts). (B) FDB muscles were cotransfected with RCaMP and NT or Mfn1siRNA. After 7 d, fibers were isolated and RCaMP-positive ones that responded to single electric pulses were picked for recording $[Ca^{2+}]_c$ and NAD(P)H transients during repetitive tetanic ES. The left graph shows a representative example of $[Ca^{2+}]_c$ transients (black) and NAD(P)H (blue) of an NTsiRNA fiber. The arrow indicates 5 µM Rotenone addition. Right: mean amplitude of the NADH levels at 30 and 150 s after the beginning of ES (n = 3 rats, the number of fibers is shown in the bar charts).

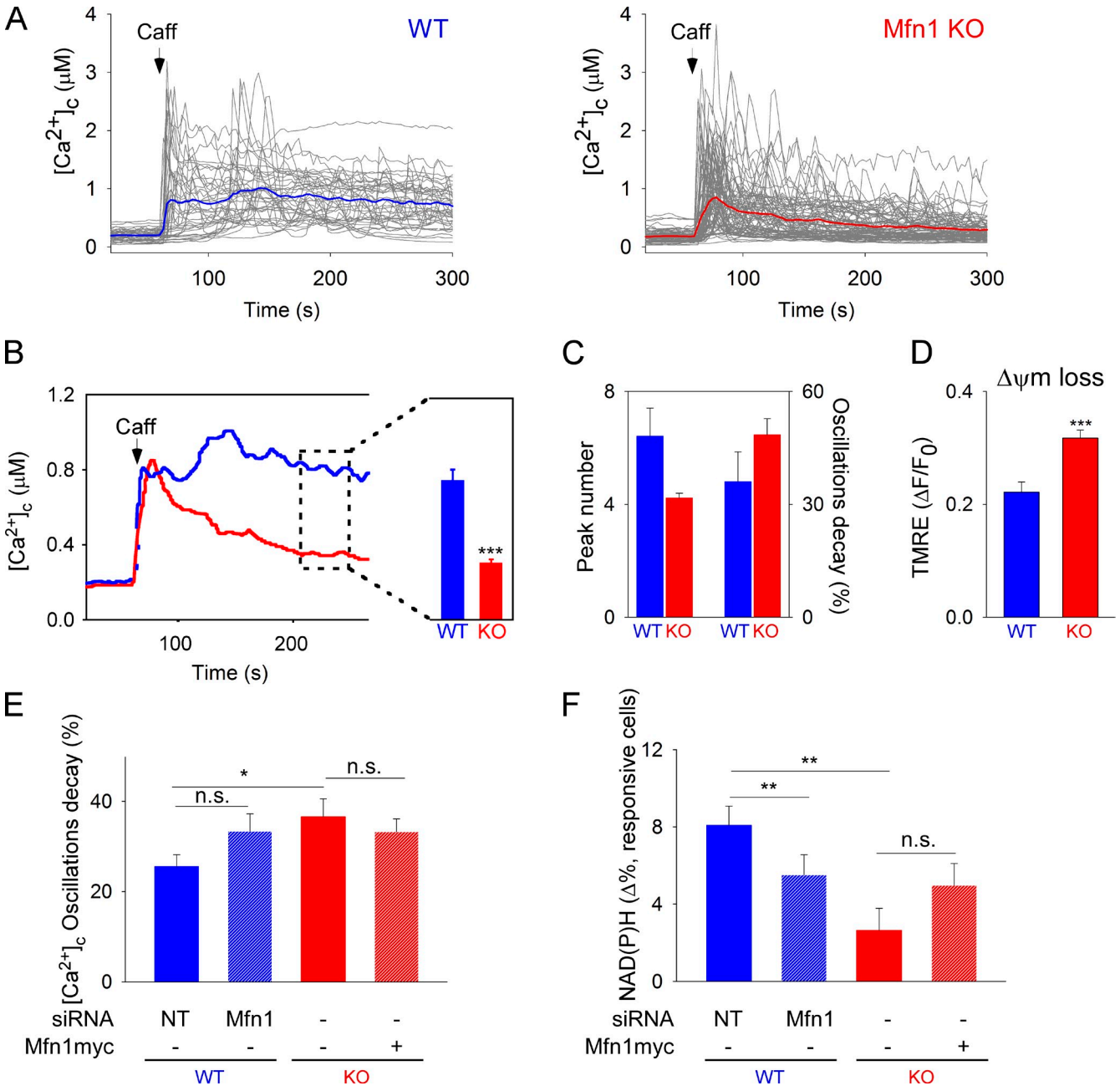

Figure 5. **Mfn1 depletion–induced perturbation of RyR1-mediated $[Ca^{2+}]_c$ oscillations, ΔΨm, and CSMDH activation.** (A) Caffeine-induced (10 mM) $[Ca^{2+}]_c$ oscillations in individual RyR1-transfected WT and Mfn1KO cells (n = 39 and 86 cells, respectively). (B) Mean time-course traces and mean $[Ca^{2+}]_c$ (200–250 s). $P < 0.001$. (C) Evaluation of the number of oscillatory peaks and oscillation amplitude decay ([peak1 − peak 3]/peak1 × 100). (D) Mitochondrial membrane potential loss 200 s after caffeine stimulation (six experiments; ***, $P < 0.001$). (E and F) MEFs were transfected with mtDsRed and RyR1 plus NTsiRNA or Mfn1 siRNA (WT), or Mfn1KO with and without Mfn1myc overexpression. Cells were stimulated with 10 mM caffeine and $[Ca^{2+}]_c$ and NAD(P)H transients were simultaneously measured. Bar charts show (E) the amplitude decay for the $[Ca^{2+}]_c$ oscillations ([peak1 − peak 3]/peak1 × 100); cell numbers: WT+NTsiRNA, n = 31; WT+Mfn1siRNA, n = 25; KO, n = 34 cells; and KO+Mfn1myc, n = 38; *, $P < 0.05$) and (F) NAD(P)H levels at 200–250 s after stimulation normalized to the baseline (cell numbers: WT+NTsiRNA, n = 95; WT+Mfn1siRNA, n = 72; KO, n = 55; and KO+Mfn1myc, n = 63; **, $P < 0.001$); n.s., not significant. Data are from four experiments.

(Fig. 7, A [middle] and D), indicating an enhanced fatigue-like response. Furthermore, 20% of the evaluated EtOH fibers display an acute decay pattern followed by an increase in $[Ca^{2+}]_c$ maintained in the post-stimulation period (Fig. 7 A, right). Also, the $[Ca^{2+}]_c$ transients of the EtOH fibers displayed uneven amplitudes during tetanic stimulation, suggesting instability of the EC-coupling and Ca^{2+}-recapturing cycles (Fig. 7 A, middle and right). The irregular $[Ca^{2+}]_c$ transient amplitude is evidenced by a high dispersion of the Ca^{2+} transient amplitude that was quantified as the difference between the maximum and the minimum peak. This irregularity in spike height is significantly higher in the fibers from the EtOH-treated animals than in their paired controls (Fig. 7 E). Because Mfn1 expression rescues SM EtOH reduced mitochondrial continuity (Fig. 6 C), we tested the effect of Mfn1 expression on $[Ca^{2+}]_c$ spiking upon repetitive tetanic stimulation. Mfn1 overexpression could not rescue $[Ca^{2+}]_c$ transients (decay

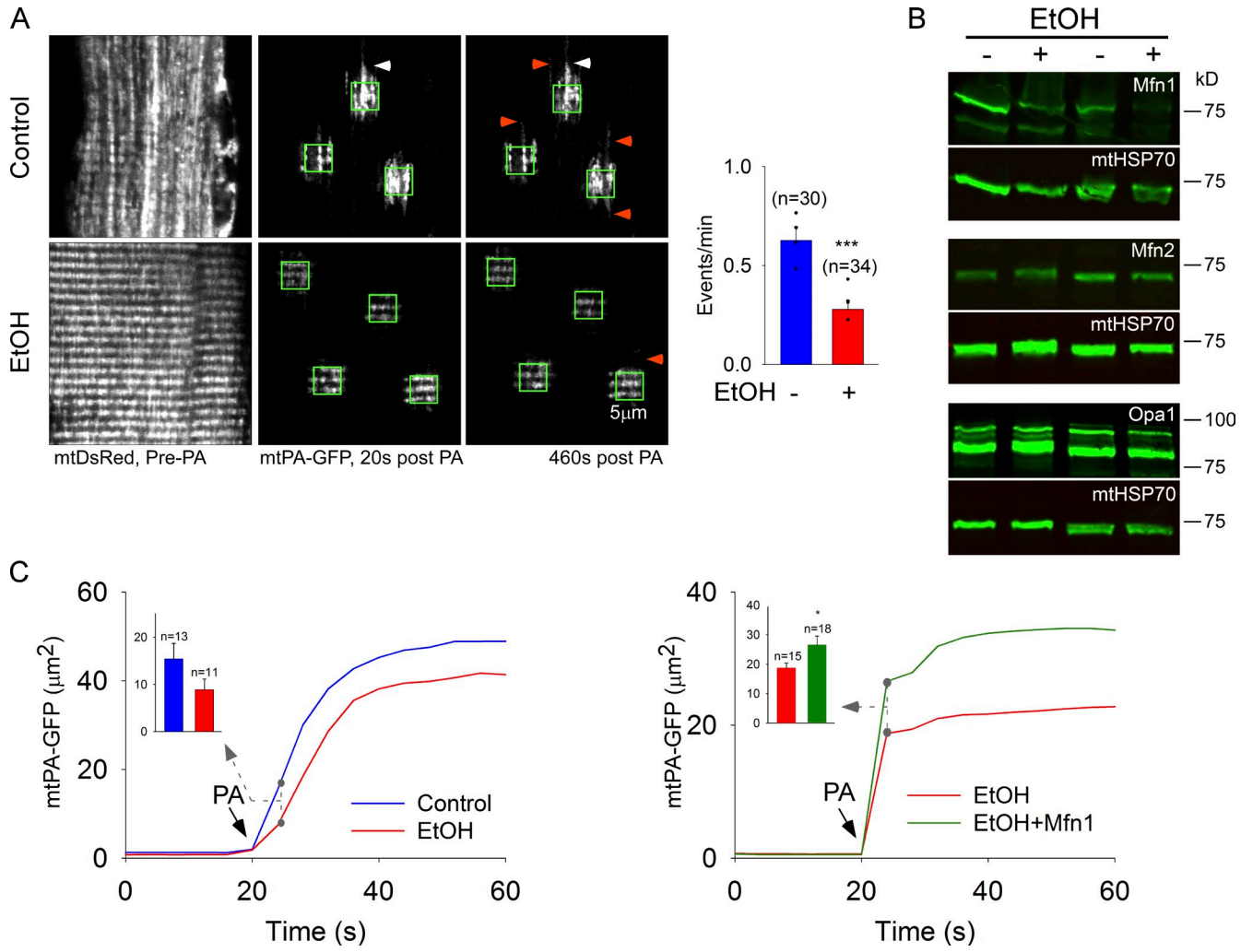

Figure 6. **Mfn1 depletion and suppression of mitochondrial fusion and continuity in fibers from EtOH-fed rats.** (A) Expression of mtDsRed and mtPA-GFP in FDB fibers harvested from EtOH-fed rats. Images show general structures of mitochondria (mtDsRed, pre-photoactivation) and organelle continuity and fusion events (mtPA-GFP, green boxes) in ethanolic- and pair-fed control fibers. White arrowheads, examples of mitochondrial continuity; orange arrowheads, fusion events. Plot on the right shows the frequency of fusion events (4 pairs of rats; ***, $P < 0.001$). (B) Mfn1, Mfn2, and Opa1 expression levels in control vs. EtOH SM mitochondria (representative of ≥9 experiments). (C) Mitochondrial continuity is attenuated by EtOH and restored by exogenous Mfn1 expression. The time course of the mtPA-GFP–positive mitochondrial area was quantified outside the region of photoactivation. Bar charts displaying mean positive area in μm^2, 4 s after photoactivation. Data from three (control vs. EtOH) and four (EtOH vs. EtOH+Mfn1; *, $P < 0.05$) experiments.

of $[Ca^{2+}]_c$ rise: 12.1 ± 2.2% EtOH vs. 11 ± 1.7% EtOH vs. EtOH+Mfn1myc). Collectively, these data indicate that chronic EtOH causes cytoplasmic calcium dysregulation that might contribute to an early fatigue-like response. The impairment of RyR1-mediated $[Ca^{2+}]_c$ transients is similar in both EtOH fibers and Mfn1 KO cells and it could not be rescued by short-term Mfn1 overexpression in either paradigm.

Despite the apparent similarity between the Mfn1 KO and chronic EtOH phenotypes of mitochondrial dynamics and RyR1-linked $[Ca^{2+}]_c$ signaling, the possibility of non–Mfn1-mediated effects of chronic EtOH should also be considered. First, the ultrastructure of the CRU, composed of the transversal tubule (TT) and the junctional sarcoplasmic reticulum (jSR), was assessed by transmission electron microscopy. The data in Table 1 show that the areas of TT and jSR, as well as the distance and contact length among them, are not altered in EtOH fibers, indicating that the CRU presents normal structural configuration. These results together with the lack of change in the initial $[Ca^{2+}]_c$ transients during pacing (Fig. 7 C) suggest that chronic EtOH did not impair CRU structure or function.

In the quantification of ultrastructure, the SR–mitochondrial gap width is unaltered but the SR–mitochondrial contact length is shortened (Table 1). Also, mitochondria display a significant increase in the area and aspect ratio (Table 1 and Fig. S5). The decrease in SR–mitochondrial contact length might be a consequence of a higher curvature of the mitochondria and it might affect the SR–mitochondrial Ca^{2+} transfer. However, the amplitude of $[Ca^{2+}]_c$ and $[Ca^{2+}]_m$ transients measured simultaneously in intact fibers showed no significant difference between control and EtOH conditions (Table 1). Therefore, we reasoned that impaired mitochondrial Ca^{2+} handling might be the link between EtOH-induced mitochondrial fusion inhibition and intracellular Ca^{2+} dysregulation. Thus, we evaluated Ca^{2+} uptake by mitochondria isolated from SM of control and EtOH-fed animals. Fig. 7 F shows that

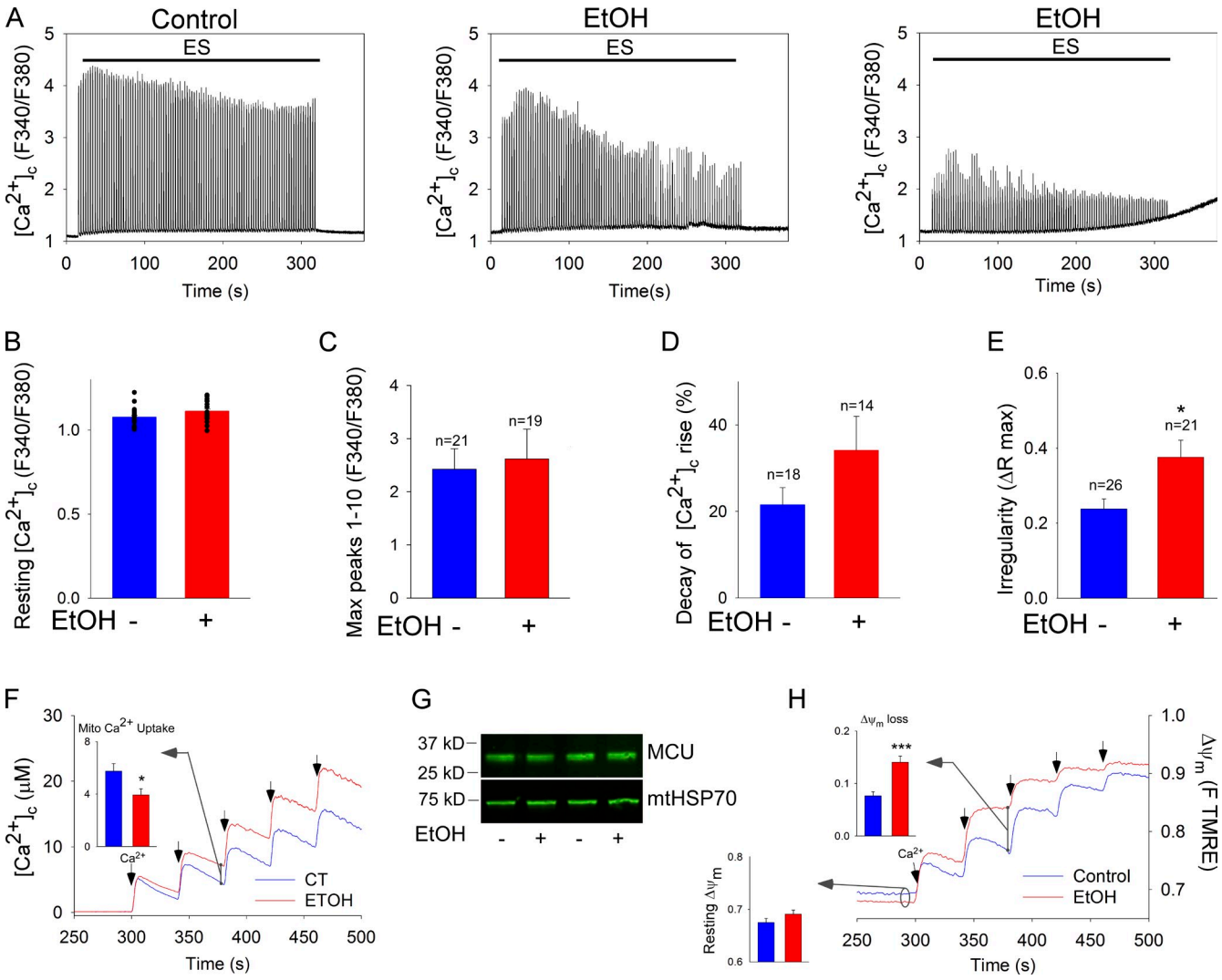

Figure 7. **Dysregulation of calcium signaling by chronic EtOH.** (A) FDB fibers were loaded with Fura2 and challenged by repetitive tetanic ES. Graphs show examples of $[Ca^{2+}]_c$ transients of a control fiber (left) and two EtOH fibers (middle and right); at least 20 fibers per condition from three experiments. (B) Resting $[Ca^{2+}]_c$ levels preES. Each fiber is represented by a dot. (C) Mean amplitude of peaks 1–10. (D) $[Ca^{2+}]_c$ transient amplitude decay (([mean peaks 1–10] − [mean peaks 30–40])/[mean peaks 1–10] × 100). (E) Irregularity in amplitude of the $[Ca^{2+}]_c$ transients ([max − min]/[max]) among peaks 1–40. *, $P < 0.05$; $n = 3$. (F) Clearance of Ca^{2+} by mitochondria. Mitochondria isolated from TA muscle of control and EtOH-fed rats were challenged by repetitive $CaCl_2$ pulses (50 μM each). Ca^{2+} uptake is shown in the representative traces by the decay of the $[Ca^{2+}]$ increases evoked by each $CaCl_2$ addition (arrows). Inset shows the mean mitochondrial Ca^{2+} uptake after the second Ca^{2+} pulse evaluated as the ruthenium red sensitive decay (4 pairs of rats; *, $P < 0.05$). (G) MCU expression levels in control vs. EtOH SM mitochondria (representative of seven experiments). (H) ΔΨm measured using TMRE. Increase in fluorescence after each $CaCl_2$ pulse indicates depolarization. Bottom inset shows resting ΔΨm as initial TMRE fluorescence normalized to the fluorescence attained after complete depolarization by uncoupler (5 μM FCCP). Top inset shows the depolarization evoked by the second pulse (8 and 4 pairs of rats, respectively; ***, $P < 0.001$).

upon repetitive $CaCl_2$ bolus additions, the clearance of Ca^{2+} by the mitochondria derived from EtOH-fed animals is suppressed. The impaired Ca^{2+} uptake does not result from down-regulation of the uniporter because the amount of the pore forming protein of the uniporter (MCU) is unchanged (Fig. 7 G). The resting mitochondrial membrane potential that is the dominant component of the driving force of Ca^{2+} uptake is also similar in ethanolic and control fibers (Fig. 7 H). However, upon repeated Ca^{2+} additions, ethanolic mitochondria display significantly more depolarization than the control organelles. An inhibitor of the mitochondrial permeability transition pore (PTP), cyclosporine A (CSA), attenuated the depolarization induced by repetitive Ca^{2+} additions in isolated mitochondria, suggesting a PTP-dependent component being involved. However, the effect of CSA was not more in ethanolic mitochondria (unpublished data). Like in intact fibers the cytoplasmic calcium dysregulation, the impaired mitochondrial Ca^{2+} handling, and membrane potential became more apparent with the repetition of stimulation. Therefore, it is plausible that the oxidative metabolism of the ethanolic mitochondria is less competent to meet challenges because their fusion-mediated quality control is ineffective. Taken together, these data support the idea that the intracellular Ca^{2+} dysregulation found in the FDB fibers of chronic EtOH-fed rats may be explained at least partially by impaired mitochondrial Ca^{2+} handling. Because the calcium phenotypes seem to reflect the capacity to maintain the driving force of mitochondrial uptake, one of the possible explanations is

Table 1. **Quantitative evaluation of CRU and mitochondrial ultrastructure, and calcium signaling in SM derived from control and EtOH-fed rats**

Animal feeding	Ultrastructural measurements								Ca^{2+} signaling	
	TT	jSR	TT-SR		Mitochondria		Mito-SR		$[Ca^{2+}]_c$	$[Ca^{2+}]_m$
	Area	Area	Gap	Contact length	Area	Aspect ratio	Gap	Contact length	Fura2 $\Delta R/R_0$	mtRCaMP $\Delta F/F_0$
	$nm^2 \times 10^{-4}$	$nm^2 \times 10^{-4}$	nm	%	$nm^2 \times 10^{-4}$		nm	nm		
Control	0.24 ± 0.01	0.8 ± 0.07	19.9 ± 0.4	70.5 ± 1.2	3.6 ± 0.3	1.33 ± 0.02	25.1 ± 1	104 ± 6	1.93 ± 0.4 (n = 10)	1.01 ± 0.3 (n = 6)
EtOH	0.22 ± 0.01	0.76 ± 0.03	18.8 ± 0.4*	68.6 ± 1.3	5.7 ± 0.5*	1.26 ± 0.02**	29.7 ± 1	83.4 ± 4**	2.19 ± 0.2 (n = 11)	0.84 ± 0.2 (n = 9)

TEM samples from FDB muscle of three pairs for control vs. EtOH-fed animals, 21,000× images, from at least three fibers and a total of 32 measurements per sample, mean ± SE. *, P < 0.03; **, P < 0.006. Calcium signaling: amplitude of one Ca^{2+} transient triggered by field stimulation (100 Hz, 500 ms, 2-ms/pulse), mean ± SE.

that depletion of the mitochondrial metabolic reserve is not instantaneous after fusion is arrested and regaining of the normal metabolic fitness is also time consuming when fusion is restored.

Discussion

In this work, we have demonstrated that in SM, mitochondria undergo dynamic fusion events and form stable connections, which are essential for normal contractile function and are likely targets of disease-causing agents. Compared with less differentiated muscle cells, the fusion events are less frequent and more stable in muscle fibers, indicating adaptation of the fusion–fission machinery to the highly organized environment and contractile forces. Fusion is primarily mediated by Mfn1 and Opa1. Loss or dominant-negative mutation of these proteins, as well as chronic alcohol exposure that induces Mfn1 depletion, suppresses mitochondrial fusion in muscle fibers. Although short-term interference with fusion does not seem to harm EC coupling, a prolonged decrease in fusion compromises mitochondrial energy metabolism and calcium oscillations that drive contractions. This occurs at least in part because suboptimal complementation leads to lesser metabolic fitness of the mitochondria, which progressively hinders calcium cycling during trains of stimulation.

Several studies have established mitochondrial fusion in yeast and eukaryotic cell lines (Hoppins and Nunnari, 2009; Chen and Chan, 2010; Westermann, 2010); however, mitochondrial fusion dynamics studies in terminally differentiated primary cells are still a work in progress. Advances have been achieved in neurons (Karbowski et al., 2004) and lately in hepatocytes (Das et al., 2012) and ventricular cardiomyocytes (Huang et al., 2013), and functional significance of the fusion proteins Mfn1/2 in both heart (Chen et al., 2011) and muscle (Chen et al., 2010) has been reported. Furthermore, mitochondrial connectivity in the adult SM has been implied based on electron microscopic visualization in fixed samples of mouse soleus (Picard et al., 2013) and the spatial distribution of cYFP flashes in live fibers (Pouvreau, 2010; Wei et al., 2011). However, this is the first study in which mitochondrial continuity and fusion are directly visualized and quantified in live SM fibers. Diffusion of mitochondrial matrix–targeted soluble PA-GFP has unveiled (1) dynamic mitochondrial networks with matrix continuity that allows permanent mtPA-GFP equilibration and (2) actual fusion events among neighboring mitochondria characterized by single-step mtPA-GFP and mtDsRed diffusion.

Muscle cell mitochondria reach different levels of organization during muscle development. We have previously demonstrated in a muscle-derived cell line (H9c2) that the elongated and greatly interconnected myoblast mitochondria transition to a more fragmented and dense mitochondrial phenotype during differentiation to myotubes (Yi et al., 2012). Similarly, FDB muscles from 0.5- to 1-mo-old mice display elongated and less organized mitochondrial distribution than adult mice muscle fibers, where mostly globular intermyofibrillar mitochondria are positioned to the I band in close proximity with SR and T-tubules forming triads (Boncompagni et al., 2009). Furthermore, inhibition of Drp1-mediated mitochondrial fission in early stages of myogenic differentiation has been reported (De Palma et al., 2010). Here, we showed that fusion events become less frequent but commonly result in long-lasting and specialized matrix complementation domains in fully differentiated SM fibers. These changes in intermitochondrial encounters can be attributed at least in part to the highly organized architecture of the muscle fiber, which offers little opportunity for mitochondrial movements to bring together and separate from other individual mitochondria (Liu et al., 2009; Twig et al., 2010). The above-described differences in both fusion and motility can be best appreciated in the time-lapse recordings (myotube [Video 2] vs. FDB fiber [Video 1]). Overall, our observations indicate that mitochondrial motility, a significant component of mitochondrial dynamics, is scarce in the adult fibers and did not play a major role in the establishment of mitochondria fusion events that mostly occurred among neighboring mitochondria. An important novel aspect of some of the stable interactions described here is their appearance as narrow connectors, which support relatively slow matrix mixing. Considering the stable nature of these connectors, they likely provide for effective complementation. It is probable that the spatial restrictions contribute to the shaping of the connectors together with some special arrangements of the components of the mitochondrial membrane. Thus, despite the transition of mitochondria to globular and spatially separated structures during SM differentiation, dynamic and some specialized forms of membrane merging maintain complementation of mitochondrial content in fully differentiated fibers.

The alteration of fusion protein expression levels or mutations leads to neurodegenerative disorders such as Charcot-Marie-Tooth type 2 (CMT2) and ADOA associated to Mfn2 and Opa1 mutations, respectively. Interestingly, ADOA and CMT2 patients also develop myopathy (Yu-Wai-Man et al., 2010; Feely et al., 2011; Vital and Vital, 2012). Muscles from ADOA adult patients, carrying Opa1 mutations, display reduced mitochondrial ATP synthesis, suggesting mitochondrial metabolism dysregulation (Lodi et al., 2011). Here, we show that the expression of ADOA-associated Opa1 mutants in vivo in the muscle fibers of adult rats compromises the mitochondria fusion dynamics, providing some clues that Opa1 mutations might cripple muscle function through inhibition of mitochondrial dynamics. However, short-term Opa1 G300E overexpression suppressed mitochondrial fusion without impairing intracellular Ca^{2+} regulation in the muscle. Notably, in some cell culture paradigms, short-term Opa1 silencing has been described to cause massive mitochondrial distortion and both increased and decreased mitochondrial Ca^{2+} uptake (Fülöp et al., 2011; Kushnareva et al., 2013). The early appearance of defects in calcium signaling might be because of a faster mitochondrial turnover in these cell types.

In SM, relatively low Mfn1 mRNA levels were reported (Santel et al., 2003). However, our results show that silencing of Mfn1 but not Mfn2 leads to greatly decreased mitochondrial connectivity and fusion activity in FDB muscle, indicating a dominant role for Mfn1. Yet, short-term Mfn1 silencing did not alter $[Ca^{2+}]_c$ transients and the ensuing increase in mitochondrial NAD(P)H in FDB fibers and had only a small effect on NAD(P)H in MEFs, in which Mfn1 is also the primary fusion protein (Chen et al., 2005). However, sustained loss of Mfn1 in KO MEFs induced dysregulation of the mitochondrial membrane potential and Ca^{2+} handling during prolonged calcium oscillations. Similarly, Chen et al. (2010) showed that in conditional Mfn1 KO mice, accumulation of mtDNA deletions in the SM happened only in old animals, suggesting that long-term down-regulation of Mfn1 is needed to induce mitochondrial damage. The loss of fusion jeopardizes complementation among mitochondria, leading to a slow decay in the respiratory complex activity that might manifest first as a decreased capacity to produce energy and handle calcium during sustained muscle activity. This, in turn, causes cytoplasmic calcium dysregulation and decreased fatigue tolerance.

Chronic ethanol consumption leads to muscle weakness (Estruch et al., 1998). Satellite cells of chronic alcoholic individuals give rise to skeletal myotubes that show attenuated Ca^{2+} transients compared with their control counterparts (Nicolás et al., 1998). Extending these data, we found that FDB fibers coming from EtOH-fed animals displayed irregular transients and rapidly decaying $[Ca^{2+}]_c$ oscillations during trains of tetanic ES. Although mitochondrial dynamics has not been considered before as the source of EtOH-induced Ca^{2+} dysregulation, multiple hints have indicated this possibility. Mitochondria provide ATP and strategically positioned Ca^{2+} feedback mechanisms that are required for normal Ca^{2+} cycling in the muscle and other cell types (Jouaville et al., 1995; Shkryl and Shirokova, 2006; Caputo and Bolaños, 2008; Weiss et al., 2010; Zhou et al., 2010), and oxidative metabolism fails when mitochondrial fusion proteins Mfn1 and 2 are knocked down (Chen et al., 2010). Also, mitochondria represent a major target of EtOH and loose their normal shape upon persistent EtOH exposure (Song and Rubin, 1972). Indeed, our study demonstrated that chronic EtOH exposure caused inhibition of mitochondrial fusion and this can be attributed, at least in part, to Mfn1 down-regulation. Furthermore, the present work showed that chronically Mfn1-deleted MEFs copy the Ca^{2+} phenotype of the ethanolic muscle fibers. In addition, both prolonged EtOH and Mfn1 KO resulted in progressive loss of the mitochondrial membrane potential during repetitive Ca^{2+} stimulation. Notably, short-term Mfn1 re-expression was sufficient to restore mitochondrial fusion in both chronic EtOH and Mfn1 KO, but failed to rescue full bioenergetic capacity at the same time. We could also show that the CRU function and SR-mitochondrial Ca^{2+} transfer were maintained in ethanolic fibers (Table 1). Collectively, our data suggest that chronic inhibition of mitochondrial fusion is detrimental to the mitochondrial quality control machinery, leading to organelles with less reserve capacity to support calcium regulation. The possibility of a similar pathomechanism in the SM of ADOA patients is indicated by our results showing fusion inhibition in mutated Opa1 expressing fibers and by the decreased SM ATP levels in ADOA patients (Lodi et al., 2011).

In conclusion, our study brings to light the mitochondrial fusion dynamics in SM and its significance in the homeostatic control of Ca^{2+} signaling during prolonged activity. From this work, mitochondrial fusion dynamics also emerges as a factor that might play a role in the development of myopathies caused by some genetic impairments and prolonged exposure to environmental cues.

Materials and methods

cDNA and siRNA constructs

The following cDNA constructs were used: mtDsRed (Takara Bio Inc.) and mtPA-GFP (Karbowski et al., 2004; Liu et al., 2009), which used the targeting sequence of cytochrome c oxidase subunit VIII, pCRII-Opa1G300E, and pCRII-Opa1 Δ58 (Olichon et al., 2007); rabbit skeletal muscle full-length pRRS11-RyR1 (Bhat et al., 1997), pcDNA3.1(−)/Myc-His-Mfn1 (Chen et al., 2003), and pRSETa-RCaMP (Akerboom et al., 2013). Rat Mfn1 or Mfn2-specific siRNA ON-TARGET plus SMARTpool and nontargeting (NT) siRNA were from Thermo Fisher Scientific.

Animal treatment

Adult male Sprague Dawley rats were fed with a nutritionally adequate liquid diet that contained EtOH as 36% of total calories for 6–11 months. Pair-fed control littermates received a liquid diet in which EtOH was isocalorically replaced with maltose-dextran (Das et al., 2012).

In vivo electroporation and FDB fiber culture

Transfection of plasmids in FDB muscles of adult rats was performed as described previously (DiFranco et al., 2009). In brief, the animals were anesthetized using 5% isoflurane to inject their footpads with 2 mg/ml hyaluronidase type IV (Sigma-Aldrich), and 1 h later, 40–60 µg total cDNA was injected (20–40 µl) followed by electroporation using acupuncture needles as electrodes and delivering 20 pulses of 100 V and 30-ms duration at 1 Hz using a square pulse stimulator (model SD9; Grass Technologies) combined with an oscilloscope (model TDS 220; Tektronix). Mfn1 or Mfn2 silencing was performed by injection of the fluorescent proteins expressing cDNAs, plus 400 pmol of siRNA. In every experiment, NT-siRNA was injected to the left footpad and Mnf1 or Mfn2 siRNA to the right footpad. 7–10 d after electroporation, the animals were euthanized and the FDB muscles were harvested. FDB muscles were digested using 3 mg/ml collagenase type 2 (Worthington Biochemical Corporation) for 2–3 h at 37°C under agitation, followed by mechanical dissociation, adapted from Casas et al. (2010). Isolated fibers were plated onto CELL-TAK–coated (BD) coverslips in DMEM/F12 medium (Lonza) supplemented with penicillin/streptomycin and 10% horse serum (HS), and used within 24 h after plating.

Cell lines, cultures, and transfections

H9c2 cells (ATCC), WT, and Mfn1KO MEF cell lines (provided by David Chan, California Institute of Technology, Pasadena, CA) were grown in DMEM (ATCC) and 10% FBS (Gibco), supplemented with penicillin/streptomycin, L-glutamine, and sodium pyruvate. Transfection of 10–30 µg of plasmid DNA was performed by electroporation (BTX Harvard Apparatus).

HUSM cultures were established from the medical waste of SM biopsies (provided by Henry Rosenberg, Thomas Jefferson University, Philadelphia, PA) taken for in vitro contracture test with the approval of the Institutional Review Board (protocol no. 01.0601). The cells were cultured in DMEM, 20% FBS (Gibco), penicillin/streptomycin, L-glutamine, and sodium pyruvate; once reaching 80% confluence, the media was replaced by identical medium supplemented with 2% FBS to allow differentiation into myotubes. Cell cultures were validated by immunostaining for muscle cell–specific desmin and RyR1. 1,000,000 HUSM cells were transfected using the Nucleofector kit for human dermal fibroblasts (Lonza) with 4–15 µg of plasmid DNA.

Rat myotubes were obtained by differentiating the satellite cells present with rat FDB fibers plated onto polylysine-coated (Sigma-Aldrich) and laminin-coated (Invitrogen) coverslips (100 µg/ml each; ∼20 coverslips/rat). The samples were infected in serum-free culture medium overnight with the adenoviruses AdmtDsRed and AdmtPA-GFP (8×10^8 particles each; Vector BioLabs). The culture was kept on 10% HS DMEM/F12 medium until day 3, and then switched to differentiating medium (2% HS). Myotubes showing 2–4 nuclei were imaged on day 4.

Mitochondria preparation

Tibialis anterior (TA) mitochondria were isolated as described previously (Frezza et al., 2007). In brief, after decapitation TA was cold-minced, and treated with PBS supplemented with 0.05% trypsin and 10 mM EDTA for 30 min. The samples were centrifuged for 5 min at 200 *g* and the pellet was resuspended in 1:5 to 1:10 volumes of buffer 1 (67 mM sucrose, 50 mM Tris-HCl, 50 mM KCl, 10 mM EDTA, and 0.2% BSA, pH 7.4) followed by homogenization at 1,200 rpm (8 strokes) and centrifugation at 700 *g*. The supernatant was centrifuged at 8,000 *g* for 10 min, and the pellet was resuspended in 5 ml of buffer 2 (250 mM sucrose, 100 µM EGTA, and 10 mM Tris-HCl, pH 7.4). The last step was repeated and the final pellet was resuspended in minimum volume of buffer 2. All steps were performed at 4°C.

Live-cell imaging

Imaging measurements were performed in a 0.25% BSA–extracellular medium (ECM) consisting of 121 mM NaCl, 5 mM $NaHCO_3$, 4.7 mM KCl, 1.2 mM KH_2PO_4, 1.2 mM $MgSO_4$, 2 mM $CaCl_2$, 10 mM glucose, and 10 mM Na-Hepes, pH 7.4, at 35°C.

Recordings of mtPA-GFP and mtDsRed (512 × 512 pixels) were performed using 488-nm and 568-nm (or 561) laser lines at 0.25 s^{-1}. In most cases a confocal imaging system (40×/NA 1.35, UApo 340; Radiance model; Bio-Rad Laboratories) was used as described previously (Liu et al., 2009). In other experiments, a laser-scanning system (63×/1.4 NA, Plan-Apo; model LSM 780; Carl Zeiss) equipped with GASP detectors was used. To photoactivate PA-GFP in 2P mode, a pulsed laser system (760 nm, Chameleon; Coherent, Inc.) was applied. To create 3D-like reconstructions, a sequence of images was collected from below the adherent surface up in 0.367-µm steps (18 steps, Z series). Image analysis was done in Spectralyzer imaging software (custom designed) or in Zen 2009 (Carl Zeiss).

For imaging of $[Ca^{2+}]_c$, the cells were first loaded with 2 µM Fura2/AM (TEFLabs) for 20 min at room temperature in 2.0% BSA/ECM, in the presence of 0.003% pluronic acid and 100 µM sulfinpyrazone. MEFs were subsequently also loaded with 20 nM TMRE (2 nM TMRE was also included during recording). After dye loading, the cells were rinsed with ECM (10 min for MEFs), and the coverslip was mounted to a heated (35°C) incubator chamber in ECM containing BSA (2% for FDB fibers or 0.25% for MEF cells) and sulfinpyrazone. Detection of Fura2 fluorescence (excitation 340 and 380 nm, emission 540/50 nm) in the fibers was achieved using an inverted microscope (40×, UApo340, model IX70; Olympus) fitted with a CCD camera (Evolve 512 EMCCD; Photometrics) and a high-speed wavelength switcher (Lambda DG; Sutter Instrument) under computer control, with data acquisition rate of 12 duplets/s (FluoStream system). The MEF cells were recorded using an inverted microscope (40×, DMIRE 2; Leica), UApo objective (Olympus), and a CCD camera (ProEM 1024, EMCCD; MultiFluo system; Princeton Instruments). Image triplets (excitation 340 and 380 nm for Fura and excitation 580 nm for TMRE) were obtained every 3 s using a motorized turret that was alternating between a filter cube for Fura2 (emission 540/50 nm) and TMRE (emission 630/60 nm).

For imaging $[Ca^{2+}]_m$ simultaneously with $[Ca^{2+}]_c$ in SM, mtRCaMP-transfected FDB fibers were loaded with Fura2/AM. Images (12 triplets/s) were acquired using excitation 340 and 380 nm for Fura2 and excitation 545 nm for mtRCaMP and a dual-band emission filter in the FluoStream system.

For recording NAD(P)H simultaneously with $[Ca^{2+}]_c$ in SM, cytoplasmic RCaMP-expressing FDB fibers were used. NADH autofluorescence (excitation 360/40 nm) and cytoRCaMP (excitation 545 nm) were recorded using a dual-band emission filter (#73101; Chroma Technology Corp.) with data acquisition rate of 12 duplets/s in the FluoStream system.

For recording of NAD(P)H simultaneously with $[Ca^{2+}]_c$ in MEFs, cells were cotransfected with mtDsRed, RyR1, and NTsiRNA or Mfn1siRNA and loaded with 2 µM Fluo8/AM (TEFLabs) as described previously for Fura2. Image triplets were detected at every 3 s: NAD(P)H autofluorescence (excitation 350/50, emission 460/50), Fluo8 (excitation 490/20 nm, emission 540/50 nm), and mtDsRed (excitation 580/20 nm, emission 630/60 nm) using the MultiFluo system. Cells were treated with 2 mM lithium acetoacetate 20 s before caffeine or ES to promote the oxidation of mitochondrial NAD(P)H. The complex 1 inhibitor rotenone was added at 5 µM at the end of every recording as a positive control to register the maximum NAD(P)H levels.

Electrical stimulation

Isolated FDB fibers were electrically stimulated by means of field stimulation as follows: 100 tetani, 100 Hz, for 500 ms every 2.5 s, pulse length 2 ms in a custom-made chamber (1 ml, holding two parallel platinum electrodes positioned on each side of the light path, 1 cm apart from each other) connected to a the square pulse stimulator and oscilloscope described above. The repetitive tetanus frequency was commanded by an external custom-designed microcontroller.

Analysis of mitochondrial matrix continuity

Mitochondrial matrix continuity was evaluated by two different approaches. Spreading of PA-GFP from the area of photoactivation was evaluated by masking the 5 × 5-µm areas and quantifying the time-dependent decay in the fluorescence intensity. Alternatively, the whole area outside the photoactivated areas was masked. The images were thresholded to reach a 0.1% signal-to-noise ratio. Then the pixels of the photoactivated areas were subtracted and the PA-GFP–positive pixels were counted. Image analysis was performed in Fiji/ImageJ. Only cells with the same number of photoactivated areas and no focus loss were compared.

Fluorometric measurements of mitochondrial Ca^{2+} uptake and $\Delta\Psi_m$ in suspensions of isolated SM mitochondria

Mitochondria from TA (0.5 mg/ml) were suspended in an intracellular medium (ICM) composed of 120 mM KCl, 10 mM NaCl, 1 mM KH_2PO_4, 20 mM Tris-Hepes, pH 7.2, 1 mg/ml each of antipain, leupeptin, and pepstatin containing 1 µM Fura2FF/FA (TEFLabs) and 2 µM TMRE (Invitrogen), and supplemented with 2 mM MgATP, 1 mM each of malate and pyruvate, 5 mM creatine phosphate, and 5 U/ml creatine phosphokinase. Fluorescence was monitored in a multiwavelength excitation/dual wavelength emission fluorimeter (DeltaRAM; Photon Technology International) using 340-nm and 380-nm excitation and 500-nm emission for Fura2FF and 545-nm excitation and 580-nm emission for TMRE. After addition of $CaCl_2$ pulses, 5 µM FCCP was added to dissipate the $\Delta\Psi_m$. Calibration of the $[Ca^{2+}]$ signal was performed at the end of each measurement by adding 1.5 mM $CaCl_2$ and subsequently 10 mM EGTA/TRIS at pH 8.5.

Western blotting

For Western blotting, 40 µg of TA mitochondrial fraction proteins were loaded onto each lane of a 7.5% SDS-PAGE and electrophoretically transferred to nitrocellulose filters. Filters were blocked with blocking buffer (LI-COR Biosciences) overnight, followed by incubation with primary antibodies (mouse monoclonal primary antibodies: Opa1 [BD] and mtHSP70 [Thermo Fisher Scientific]; and rabbit polyclonal antibodies: MCU [Sigma-Aldrich], Mfn1 [provided by Richard Youle, National Institutes of Health, Bethesda, MD], and Mfn2 generated against Mfn2 [710–757]-GST and N-terminal peptide CNSIVTVKKNKRIIM-OH [provided by Heidi McBride, McGill University, Montreal, Canada]). Bound antibodies were visualized by IRDye 800 secondary antibodies (LI-COR Biosciences).

Transmission electron microscopy

SM samples were prepared as described previously (Franzini-Armstrong and Boncompagni, 2011) with few modifications. In brief, control and EtOH-fed rats were killed via decapitation and whole feet without skin were fixed in 3.5% glutaraldehyde for 2 h at room temperature and overnight at 4°C. The next day, FDB muscle was dissected into small bundles of fibers, washed four times with 0.1 M sodium cacodylate buffer, and stained with

2% osmium tetroxide in 0.1 M sodium cacodylate buffer for 2 h. Then the samples were washed with water and stained with 5% uranyl acetate for 2 h. Stained samples were dehydrated on an acetone dilution series and embedded in Spurr's resin according to the manufacturer's instructions (Elecron Microscopy Sciences). 60–100-nm thin sections were cut from the embedded specimens, mounted on electron microscopy grids, and examined using a transmission electron microscope (Tecnai 12; FEI) equipped with a phosphor plate (Advanced Microscopy Techniques) and 8-megapixel digital camera (Orca; Hamamatsu Photonics).

Morphometric analysis of intermyofibrillar mitochondria, jSR, and TT was performed on longitudinal sections using Fiji/ImageJ software, adapting protocols previously described on heart (Chen et al., 2012). In brief, CRUs (triads) and the adjunct mitochondria were identified in 21,000× images and the areas and aspect ratio of TT, jSR, and mitochondria were measured. The gap between TT and jSR was calculated as the mean of three distances between organellar membranes. TT–jSR contact length represents the percentage of the TT's half perimeter that faces the SR, when the gap between the two organelles is <30 nm. jSR–mitochondria contact is expressed as length of the jSR that faces the mitochondria when the gap among organelles is <50 nm.

Statistics

The data are shown as the mean ± SE of *n* fibers of at least three independent experiments unless it is specified differently. Significance of differences was calculated by Student's *t* test.

Online supplemental material

Fig. S1 provides insight into the different modes of mitochondrial continuity in adult SM. Fig. S2 shows diversity of the spatial organization of mitochondrial fusion events in adult FDB fibers. Fig. S3 provides evidence that short-term expression of Opa1 G300E does not alter trains of $[Ca^{2+}]_c$ transients in SM fibers. Fig. S4 shows electrical stimulation–induced NAD(P)H transient in a nontransfected fiber. Fig. S5 shows TEM representative images of longitudinal sections of FDB muscles from control and EtOH-fed paired rats. Video 1 shows time-lapse imaging of adult FDB fiber mitochondrial fusion dynamics. Video 2 shows time-lapse imaging of myotube mitochondrial fusion dynamics. Online supplemental material is available at http://www.jcb.org/cgi/content/full/jcb.201312066/DC1.

We thank Pal Pacher and Christopher Buzas for initiating the HUSM cultures and George Purkins for setting up the electrical stimulation and analytical protocols, Timothy Schneider for processing TEM samples, and Julio Vergara and Marino DiFranco for their advice on rat FDB electroporation. Furthermore, we thank Jasper Akerboom, David Chan, Loren Looger, Heidi McBride, Tullio Pozzan, Rosario Rizzuto, Emanuel Rubin, Erin Seifert, Orian Shirihai, Peter Varnai, David Weaver, and Gyorgy Csordás for helpful discussions and/or reagents.

This work was supported by PEW Latin American Fellows Program in the Biomedical Sciences and the Duchenne Parent Project, Netherlands fellowships to V. Eisner, and by a National Institutes of Health grant (AA017773) to G. Hajnóczky.

The authors declare no competing financial interests.

Submitted: 16 December 2013
Accepted: 21 March 2014

References

Akerboom, J., N. Carreras Calderón, L. Tian, S. Wabnig, M. Prigge, J. Tolö, A. Gordus, M.B. Orger, K.E. Severi, J.J. Macklin, et al. 2013. Genetically encoded calcium indicators for multi-color neural activity imaging and combination with optogenetics. *Front Mol Neurosci*. 6:2. http://dx.doi.org/10.3389/fnmol.2013.00002

Amchenkova, A.A., L.E. Bakeeva, Y.S. Chentsov, V.P. Skulachev, and D.B. Zorov. 1988. Coupling membranes as energy-transmitting cables. I. Filamentous mitochondria in fibroblasts and mitochondrial clusters in cardiomyocytes. *J. Cell Biol.* 107:481–495. http://dx.doi.org/10.1083/jcb.107.2.481

Bhat, M.B., J. Zhao, W. Zang, C.W. Balke, H. Takeshima, W.G. Wier, and J. Ma. 1997. Caffeine-induced release of intracellular Ca2+ from Chinese hamster ovary cells expressing skeletal muscle ryanodine receptor. Effects on full-length and carboxyl-terminal portion of Ca2+ release channels. *J. Gen. Physiol.* 110:749–762. http://dx.doi.org/10.1085/jgp.110.6.749

Boncompagni, S., A.E. Rossi, M. Micaroni, G.V. Beznoussenko, R.S. Polishchuk, R.T. Dirksen, and F. Protasi. 2009. Mitochondria are linked to calcium stores in striated muscle by developmentally regulated tethering structures. *Mol. Biol. Cell*. 20:1058–1067. http://dx.doi.org/10.1091/mbc.E08-07-0783

Brini, M., F. De Giorgi, M. Murgia, R. Marsault, M.L. Massimino, M. Cantini, R. Rizzuto, and T. Pozzan. 1997. Subcellular analysis of Ca2+ homeostasis in primary cultures of skeletal muscle myotubes. *Mol. Biol. Cell*. 8:129–143. http://dx.doi.org/10.1091/mbc.8.1.129

Caputo, C., and P. Bolaños. 2008. Effect of mitochondria poisoning by FCCP on Ca2+ signaling in mouse skeletal muscle fibers. *Pflugers Arch.* 455:733–743. http://dx.doi.org/10.1007/s00424-007-0317-0

Casas, M., R. Figueroa, G. Jorquera, M. Escobar, J. Molgó, and E. Jaimovich. 2010. IP(3)-dependent, post-tetanic calcium transients induced by electrostimulation of adult skeletal muscle fibers. *J. Gen. Physiol.* 136:455–467. http://dx.doi.org/10.1085/jgp.200910397

Cereghetti, G.M., A. Stangherlin, O. Martins de Brito, C.R. Chang, C. Blackstone, P. Bernardi, and L. Scorrano. 2008. Dephosphorylation by calcineurin regulates translocation of Drp1 to mitochondria. *Proc. Natl. Acad. Sci. USA*. 105:15803–15808. http://dx.doi.org/10.1073/pnas.0808249105

Chen, H., and D.C. Chan. 2010. Physiological functions of mitochondrial fusion. *Ann. N. Y. Acad. Sci.* 1201:21–25. http://dx.doi.org/10.1111/j.1749-6632.2010.05615.x

Chen, H., S.A. Detmer, A.J. Ewald, E.E. Griffin, S.E. Fraser, and D.C. Chan. 2003. Mitofusins Mfn1 and Mfn2 coordinately regulate mitochondrial fusion and are essential for embryonic development. *J. Cell Biol.* 160:189–200. http://dx.doi.org/10.1083/jcb.200211046

Chen, H., A. Chomyn, and D.C. Chan. 2005. Disruption of fusion results in mitochondrial heterogeneity and dysfunction. *J. Biol. Chem.* 280:26185–26192. http://dx.doi.org/10.1074/jbc.M503062200

Chen, H., M. Vermulst, Y.E. Wang, A. Chomyn, T.A. Prolla, J.M. McCaffery, and D.C. Chan. 2010. Mitochondrial fusion is required for mtDNA stability in skeletal muscle and tolerance of mtDNA mutations. *Cell*. 141:280–289. http://dx.doi.org/10.1016/j.cell.2010.02.026

Chen, Y., Y. Liu, and G.W. Dorn II. 2011. Mitochondrial fusion is essential for organelle function and cardiac homeostasis. *Circ. Res.* 109:1327–1331. http://dx.doi.org/10.1161/CIRCRESAHA.111.258723

Chen, Y., G. Csordás, C. Jowdy, T.G. Schneider, N. Csordás, W. Wang, Y. Liu, M. Kohlhaas, M. Meiser, S. Bergem, et al. 2012. Mitofusin 2-containing mitochondrial-reticular microdomains direct rapid cardiomyocyte bioenergetic responses via interorganelle Ca(2+) crosstalk. *Circ. Res.* 111:863–875. http://dx.doi.org/10.1161/CIRCRESAHA.112.266585

Das, S., N. Hajnóczky, A.N. Antony, G. Csordás, L.D. Gaspers, D.L. Clemens, J.B. Hoek, and G. Hajnóczky. 2012. Mitochondrial morphology and dynamics in hepatocytes from normal and ethanol-fed rats. *Pflugers Arch.* 464:101–109. http://dx.doi.org/10.1007/s00424-012-1100-4

de Brito, O.M., and L. Scorrano. 2008. Mitofusin 2 tethers endoplasmic reticulum to mitochondria. *Nature*. 456:605–610. http://dx.doi.org/10.1038/nature07534

De Palma, C., S. Falcone, S. Pisoni, S. Cipolat, C. Panzeri, S. Pambianco, A. Pisconti, R. Allevi, M.T. Bassi, G. Cossu, et al. 2010. Nitric oxide inhibition of Drp1-mediated mitochondrial fission is critical for myogenic differentiation. *Cell Death Differ.* 17:1684–1696. http://dx.doi.org/10.1038/cdd.2010.48

Detmer, S.A., and D.C. Chan. 2007. Functions and dysfunctions of mitochondrial dynamics. *Nat. Rev. Mol. Cell Biol.* 8:870–879. http://dx.doi.org/10.1038/nrm2275

DiFranco, M., M. Quinonez, J. Capote, and J. Vergara. 2009. DNA transfection of mammalian skeletal muscles using in vivo electroporation. *J. Vis. Exp.* pii:1520.

Eisner, V., V. Parra, S. Lavandero, C. Hidalgo, and E. Jaimovich. 2010. Mitochondria fine-tune the slow Ca(2+) transients induced by electrical stimulation of skeletal myotubes. *Cell Calcium.* 48:358–370. http://dx.doi.org/10.1016/j.ceca.2010.11.001

Eisner, V., G. Csordás, and G. Hajnóczky. 2013. Interactions between sarco-endoplasmic reticulum and mitochondria in cardiac and skeletal muscle - pivotal roles in Ca^{2+} and reactive oxygen species signaling. *J. Cell Sci.* 126:2965–2978. http://dx.doi.org/10.1242/jcs.093609

Estruch, R., E. Sacanella, J. Fernández-Solá, J.M. Nicolás, E. Rubin, and A. Urbano-Márquez. 1998. Natural history of alcoholic myopathy: a 5-year study. *Alcohol. Clin. Exp. Res.* 22:2023–2028.

Feely, S.M., M. Laura, C.E. Siskind, S. Sottile, M. Davis, V.S. Gibbons, M.M. Reilly, and M.E. Shy. 2011. MFN2 mutations cause severe phenotypes in most patients with CMT2A. *Neurology*. 76:1690–1696. http://dx.doi.org/10.1212/WNL.0b013e31821a441e

Fernández-Solà, J., J.M. Nicolás, E. Sacanella, J. Robert, M. Cofan, R. Estruch, and A. Urbano-Márquez. 2000. Low-dose ethanol consumption allows strength recovery in chronic alcoholic myopathy. *QJM*. 93:35–40. http://dx.doi.org/10.1093/qjmed/93.1.35

Franzini-Armstrong, C., and S. Boncompagni. 2011. The evolution of the mitochondria-to-calcium release units relationship in vertebrate skeletal muscles. *J. Biomed. Biotechnol.* 2011:830573. http://dx.doi.org/10.1155/2011/830573

Frezza, C., S. Cipolat, O. Martins de Brito, M. Micaroni, G.V. Beznoussenko, T. Rudka, D. Bartoli, R.S. Polishuck, N.N. Danial, B. De Strooper, and L. Scorrano. 2006. OPA1 controls apoptotic cristae remodeling independently from mitochondrial fusion. *Cell*. 126:177–189. http://dx.doi.org/10.1016/j.cell.2006.06.025

Frezza, C., S. Cipolat, and L. Scorrano. 2007. Organelle isolation: functional mitochondria from mouse liver, muscle and cultured fibroblasts. *Nat. Protoc.* 2:287–295. http://dx.doi.org/10.1038/nprot.2006.478

Frieden, M., D. James, C. Castelbou, A. Danckaert, J.C. Martinou, and N. Demaurex. 2004. Ca(2+) homeostasis during mitochondrial fragmentation and perinuclear clustering induced by hFis1. *J. Biol. Chem.* 279:22704–22714. http://dx.doi.org/10.1074/jbc.M312366200

Fülöp, L., G. Szanda, B. Enyedi, P. Várnai, and A. Spät. 2011. The effect of OPA1 on mitochondrial Ca^{2+} signaling. *PLoS ONE*. 6:e25199. http://dx.doi.org/10.1371/journal.pone.0025199

Hajnóczky, G., L.D. Robb-Gaspers, M.B. Seitz, and A.P. Thomas. 1995. Decoding of cytosolic calcium oscillations in the mitochondria. *Cell*. 82:415–424. http://dx.doi.org/10.1016/0092-8674(95)90430-1

Hom, J.R., J.S. Gewandter, L. Michael, S.S. Sheu, and Y. Yoon. 2007. Thapsigargin induces biphasic fragmentation of mitochondria through calcium-mediated mitochondrial fission and apoptosis. *J. Cell. Physiol.* 212:498–508. http://dx.doi.org/10.1002/jcp.21051

Hoppins, S., and J. Nunnari. 2009. The molecular mechanism of mitochondrial fusion. *Biochim. Biophys. Acta*. 1793:20–26. http://dx.doi.org/10.1016/j.bbamcr.2008.07.005

Huang, X., L. Sun, S. Ji, T. Zhao, W. Zhang, J. Xu, J. Zhang, Y. Wang, X. Wang, C. Franzini-Armstrong, et al. 2013. Kissing and nanotunneling mediate intermitochondrial communication in the heart. *Proc. Natl. Acad. Sci. USA*. 110:2846–2851. http://dx.doi.org/10.1073/pnas.1300741110

Jouaville, L.S., F. Ichas, E.L. Holmuhamedov, P. Camacho, and J.D. Lechleiter. 1995. Synchronization of calcium waves by mitochondrial substrates in Xenopus laevis oocytes. *Nature*. 377:438–441. http://dx.doi.org/10.1038/377438a0

Jouaville, L.S., P. Pinton, C. Bastianutto, G.A. Rutter, and R. Rizzuto. 1999. Regulation of mitochondrial ATP synthesis by calcium: evidence for a long-term metabolic priming. *Proc. Natl. Acad. Sci. USA*. 96:13807–13812. http://dx.doi.org/10.1073/pnas.96.24.13807

Karbowski, M., and R.J. Youle. 2011. Regulating mitochondrial outer membrane proteins by ubiquitination and proteasomal degradation. *Curr. Opin. Cell Biol.* 23:476–482. http://dx.doi.org/10.1016/j.ceb.2011.05.007

Karbowski, M., D. Arnoult, H. Chen, D.C. Chan, C.L. Smith, and R.J. Youle. 2004. Quantitation of mitochondrial dynamics by photolabeling of individual organelles shows that mitochondrial fusion is blocked during the Bax activation phase of apoptosis. *J. Cell Biol.* 164:493–499. http://dx.doi.org/10.1083/jcb.200309082

Kushnareva, Y.E., A.A. Gerencser, B. Bossy, W.K. Ju, A.D. White, J. Waggoner, M.H. Ellisman, G. Perkins, and E. Bossy-Wetzel. 2013. Loss of OPA1 disturbs cellular calcium homeostasis and sensitizes for excitotoxicity. *Cell Death Differ.* 20:353–365. http://dx.doi.org/10.1038/cdd.2012.128

Lackner, L.L., and J.M. Nunnari. 2009. The molecular mechanism and cellular functions of mitochondrial division. *Biochim. Biophys. Acta*. 1792:1138–1144. http://dx.doi.org/10.1016/j.bbadis.2008.11.011

Lemasters, J.J. 2005. Selective mitochondrial autophagy, or mitophagy, as a targeted defense against oxidative stress, mitochondrial dysfunction, and aging. *Rejuvenation Res.* 8:3–5. http://dx.doi.org/10.1089/rej.2005.8.3

Liu, X., D. Weaver, O. Shirihai, and G. Hajnóczky. 2009. Mitochondrial 'kiss-and-run': interplay between mitochondrial motility and fusion-fission dynamics. *EMBO J.* 28:3074–3089. http://dx.doi.org/10.1038/emboj.2009.255

Lodi, R., C. Tonon, M.L. Valentino, D. Manners, C. Testa, E. Malucelli, C. La Morgia, P. Barboni, M. Carbonelli, S. Schimpf, et al. 2011. Defective mitochondrial adenosine triphosphate production in skeletal muscle from patients with dominant optic atrophy due to OPA1 mutations. *Arch. Neurol.* 68:67–73. http://dx.doi.org/10.1001/archneurol.2010.228

Mitchell, T., B. Chacko, S.W. Ballinger, S.M. Bailey, J. Zhang, and V. Darley-Usmar. 2013. Convergent mechanisms for dysregulation of mitochondrial quality control in metabolic disease: implications for mitochondrial therapeutics. *Biochem. Soc. Trans.* 41:127–133. http://dx.doi.org/10.1042/BST20120231

Nicolás, J.M., E. Antúnez, A.P. Thomas, J. Fernández-Solà, E. Tobías, R. Estruch, and A. Urbano-Márquez. 1998. Ethanol acutely decreases calcium transients in cultured human myotubes. *Alcohol. Clin. Exp. Res.* 22:1086–1092. http://dx.doi.org/10.1111/j.1530-0277.1998.tb03705.x

Ogata, T., and Y. Yamasaki. 1997. Ultra-high-resolution scanning electron microscopy of mitochondria and sarcoplasmic reticulum arrangement in human red, white, and intermediate muscle fibers. *Anat. Rec.* 248:214–223. http://dx.doi.org/10.1002/(SICI)1097-0185(199706)248:2<214::AID-AR8>3.0.CO;2-S

Olichon, A., T. Landes, L. Arnauné-Pelloquin, L.J. Emorine, V. Mils, A. Guichet, C. Delettre, C. Hamel, P. Amati-Bonneau, D. Bonneau, et al. 2007. Effects of OPA1 mutations on mitochondrial morphology and apoptosis: relevance to ADOA pathogenesis. *J. Cell. Physiol.* 211:423–430. http://dx.doi.org/10.1002/jcp.20950

Ono, T., K. Isobe, K. Nakada, and J.I. Hayashi. 2001. Human cells are protected from mitochondrial dysfunction by complementation of DNA products in fused mitochondria. *Nat. Genet.* 28:272–275. http://dx.doi.org/10.1038/90116

Pacher, P., A.P. Thomas, and G. Hajnóczky. 2002. Ca2+ marks: miniature calcium signals in single mitochondria driven by ryanodine receptors. *Proc. Natl. Acad. Sci. USA*. 99:2380–2385. http://dx.doi.org/10.1073/pnas.032423699

Papanicolaou, K.N., R.J. Khairallah, G.A. Ngoh, A. Chikando, I. Luptak, K.M. O'Shea, D.D. Riley, J.J. Lugus, W.S. Colucci, W.J. Lederer, et al. 2011. Mitofusin-2 maintains mitochondrial structure and contributes to stress-induced permeability transition in cardiac myocytes. *Mol. Cell. Biol.* 31:1309–1328. http://dx.doi.org/10.1128/MCB.00911-10

Partikian, A., B. Olveczky, R. Swaminathan, Y. Li, and A.S. Verkman. 1998. Rapid diffusion of green fluorescent protein in the mitochondrial matrix. *J. Cell Biol.* 140:821–829. http://dx.doi.org/10.1083/jcb.140.4.821

Picard, M., K. White, and D.M. Turnbull. 2013. Mitochondrial morphology, topology, and membrane interactions in skeletal muscle: a quantitative three-dimensional electron microscopy study. *J. Appl. Physiol.* 114:161–171. http://dx.doi.org/10.1152/japplphysiol.01096.2012

Pouvreau, S. 2010. Superoxide flashes in mouse skeletal muscle are produced by discrete arrays of active mitochondria operating coherently. *PLoS ONE*. 5:e13035. http://dx.doi.org/10.1371/journal.pone.0013035

Rizzuto, R., C. Bastianutto, M. Brini, M. Murgia, and T. Pozzan. 1994. Mitochondrial Ca2+ homeostasis in intact cells. *J. Cell Biol.* 126:1183–1194. http://dx.doi.org/10.1083/jcb.126.5.1183

Robb-Gaspers, L.D., P. Burnett, G.A. Rutter, R.M. Denton, R. Rizzuto, and A.P. Thomas. 1998. Integrating cytosolic calcium signals into mitochondrial metabolic responses. *EMBO J.* 17:4987–5000. http://dx.doi.org/10.1093/emboj/17.17.4987

Rogers, K.L., S. Picaud, E. Roncali, R. Boisgard, C. Colasante, J. Stinnakre, B. Tavitian, and P. Brûlet. 2007. Non-invasive in vivo imaging of calcium signaling in mice. *PLoS ONE*. 2:e974. http://dx.doi.org/10.1371/journal.pone.0000974

Rossi, A.E., S. Boncompagni, L. Wei, F. Protasi, and R.T. Dirksen. 2011. Differential impact of mitochondrial positioning on mitochondrial Ca(2+) uptake and Ca(2+) spark suppression in skeletal muscle. *Am. J. Physiol. Cell Physiol.* 301:C1128–C1139. http://dx.doi.org/10.1152/ajpcell.00194.2011

Rudolf, R., M. Mongillo, P.J. Magalhães, and T. Pozzan. 2004. In vivo monitoring of Ca(2+) uptake into mitochondria of mouse skeletal muscle during contraction. *J. Cell Biol.* 166:527–536. http://dx.doi.org/10.1083/jcb.200403102

Santel, A., S. Frank, B. Gaume, M. Herrler, R.J. Youle, and M.T. Fuller. 2003. Mitofusin-1 protein is a generally expressed mediator of mitochondrial fusion in mammalian cells. *J. Cell Sci.* 116:2763–2774. http://dx.doi.org/10.1242/jcs.00479

Shkryl, V.M., and N. Shirokova. 2006. Transfer and tunneling of Ca2+ from sarcoplasmic reticulum to mitochondria in skeletal muscle. *J. Biol. Chem.* 281:1547–1554. http://dx.doi.org/10.1074/jbc.M505024200

Song, S.K., and E. Rubin. 1972. Ethanol produces muscle damage in human volunteers. *Science*. 175:327–328. http://dx.doi.org/10.1126/science.175.4019.327

Szabadkai, G., A.M. Simoni, M. Chami, M.R. Wieckowski, R.J. Youle, and R. Rizzuto. 2004. Drp-1-dependent division of the mitochondrial network blocks intraorganellar Ca2+ waves and protects against Ca2+-mediated apoptosis. *Mol. Cell*. 16:59–68. http://dx.doi.org/10.1016/j.molcel.2004.09.026

Tatsuta, T., and T. Langer. 2008. Quality control of mitochondria: protection against neurodegeneration and ageing. *EMBO J.* 27:306–314. http://dx.doi.org/10.1038/sj.emboj.7601972

Twig, G., A. Elorza, A.J. Molina, H. Mohamed, J.D. Wikstrom, G. Walzer, L. Stiles, S.E. Haigh, S. Katz, G. Las, et al. 2008. Fission and selective fusion govern mitochondrial segregation and elimination by autophagy. *EMBO J.* 27:433–446. http://dx.doi.org/10.1038/sj.emboj.7601963

Twig, G., X. Liu, M. Liesa, J.D. Wikstrom, A.J. Molina, G. Las, G. Yaniv, G. Hajnóczky, and O.S. Shirihai. 2010. Biophysical properties of mitochondrial fusion events in pancreatic beta-cells and cardiac cells unravel potential control mechanisms of its selectivity. *Am. J. Physiol. Cell Physiol.* 299:C477–C487. http://dx.doi.org/10.1152/ajpcell.00427.2009

Vendelin, M., N. Béraud, K. Guerrero, T. Andrienko, A.V. Kuznetsov, J. Olivares, L. Kay, and V.A. Saks. 2005. Mitochondrial regular arrangement in muscle cells: a "crystal-like" pattern. *Am. J. Physiol. Cell Physiol.* 288:C757–C767. http://dx.doi.org/10.1152/ajpcell.00281.2004

Vital, A., and C. Vital. 2012. Mitochondria and peripheral neuropathies. *J. Neuropathol. Exp. Neurol.* 71:1036–1046. http://dx.doi.org/10.1097/NEN.0b013e3182764d47

Wei, L., G. Salahura, S. Boncompagni, K.A. Kasischke, F. Protasi, S.S. Sheu, and R.T. Dirksen. 2011. Mitochondrial superoxide flashes: metabolic biomarkers of skeletal muscle activity and disease. *FASEB J.* 25:3068–3078. http://dx.doi.org/10.1096/fj.11-187252

Weiss, N., T. Andrianjafiniony, S. Dupré-Aucouturier, S. Pouvreau, D. Desplanches, and V. Jacquemond. 2010. Altered myoplasmic Ca(2+) handling in rat fast-twitch skeletal muscle fibres during disuse atrophy. *Pflugers Arch.* 459:631–644. http://dx.doi.org/10.1007/s00424-009-0764-x

Westerblad, H., J.A. Lee, J. Lännergren, and D.G. Allen. 1991. Cellular mechanisms of fatigue in skeletal muscle. *Am. J. Physiol.* 261:C195–C209.

Westermann, B. 2010. Mitochondrial fusion and fission in cell life and death. *Nat. Rev. Mol. Cell Biol.* 11:872–884. http://dx.doi.org/10.1038/nrm3013

Yi, M., D. Weaver, V. Eisner, P. Várnai, L. Hunyady, J. Ma, G. Csordás, and G. Hajnóczky. 2012. Switch from ER-mitochondrial to SR-mitochondrial calcium coupling during muscle differentiation. *Cell Calcium*. 52:355–365. http://dx.doi.org/10.1016/j.ceca.2012.05.012

Yu-Wai-Man, P., P.G. Griffiths, G.S. Gorman, C.M. Lourenco, A.F. Wright, M. Auer-Grumbach, A. Toscano, O. Musumeci, M.L. Valentino, L. Caporali, et al. 2010. Multi-system neurological disease is common in patients with OPA1 mutations. *Brain*. 133:771–786. http://dx.doi.org/10.1093/brain/awq007

Zhou, J., J. Yi, R. Fu, E. Liu, T. Siddique, E. Ríos, and H.X. Deng. 2010. Hyperactive intracellular calcium signaling associated with localized mitochondrial defects in skeletal muscle of an animal model of amyotrophic lateral sclerosis. *J. Biol. Chem.* 285:705–712. http://dx.doi.org/10.1074/jbc.M109.041319